Holocene-like summer climate during Marine Isotope Stage 11 in northwestern Greenland

John Michael N. Aguilar[1,2], Elizabeth K. Thomas[1]*, Diana S. Aga[2], Paul R. Bierman[3,4], Jason P. Briner[1], Isla S. Castañeda[5], Andrew J. Christ[3,a]

[1]Department of Earth Sciences, University at Buffalo, The State University of New York, Buffalo, NY, 14260, USA

[2]Department of Chemistry, University at Buffalo, The State of University of New York, Buffalo, NY, 14260, USA

[3]Rubenstein School of the Environment and Natural Resources, University of Vermont, Burlington, VT 05401, USA

[4]Gund Institute for Environment, University of Vermont, Burlington, VT 05401, USA

[5]Department of Earth, Geographic and Climate Sciences, University of Massachusetts, Amherst, MA 01002, USA

[a]currently at: U.S. Reinsurance Analytics, Aon plc, Denver, CO 80206, USA

*Corresponding author: Elizabeth K. Thomas (ekthomas@buffalo.edu)

Key Points:

1. MIS 11 in northwestern Greenland had similar summer temperature to peak Holocene conditions across Greenland
2. Holocene-like MIS 11 conditions suggest that sustained moderate warmth can drive major Greenland Ice Sheet loss
3. ^{2}H-enriched summer vapor during MIS 11 due to greater local evapotranspiration, consistent with reduced ice extent and expanded vegetation

Keywords: Camp Century, Marine Isotope Stage 11, Greenland Ice Sheet

Abstract

Determining the climatic conditions under which the Greenland Ice Sheet (GrIS) was smaller than present is important to quantify GrIS sensitivity to climate change. We use biomarkers in sediment collected beneath the GrIS at Camp Century, northwestern Greenland, to reconstruct summer temperature and atmospheric circulation 416,000 ± 38,000 years ago, at some point during Marine Isotope Stage 11 (MIS 11). We find that northwestern Greenland summer climate during MIS 11 was similar to the middle Holocene but different than the 20^{th} century. Air temperature was 4.7 ± 3.2°C warmer, and atmospheric water vapor isotope values were 22 ± 18 ‰ ^{2}H-enriched, indicating a greater contribution of locally evapotranspired moisture. These conditions are similar to or slightly warmer than during peak Holocene warmth on Greenland, when the Camp Century site remained ice-covered, and cooler than the Last Interglacial (LIG). Biomarkers from lower in the section likely represent an earlier ice-free interval, potentially during the Pliocene or early Pleistocene, and record climatic conditions similar to MIS 11. These data add to the sparse available climate data for the early and middle Pleistocene on Greenland, and suggest interglacial periods had similar temperature throughout the Pleistocene. We interpret the reduced GrIS extent in northwestern Greenland during MIS11 compared to the Holocene, despite similar temperature, to indicate ice-sheet response to prolonged warmth, as reconstructed in southern Greenland. Therefore, efforts to reduce both the magnitude and duration of summer warmth in the coming centuries will be important to curbing ice-sheet retreat.

1. Introduction

Quantifying the sensitivity of the Greenland Ice Sheet (GrIS) to climate is an important challenge, as the GrIS contains 7.4 m sea level equivalent and the Arctic is in a rapidly warming part of the planet (Aschwanden et al., 2019; Smith et al., 2020). Ocean warming may cause rapid recession of calving glaciers, some of which are sourced from near the center of the GrIS (Callard et al., 2025; Guo et al., 2019; Holland et al., 2008). Yet, much of the GrIS bed is above sea level and should be resilient to ocean forcing (Morlighem et al., 2017). While increased atmospheric warming also causes ice-sheet mass loss and greater snowfall may partially offset this melt, the elevation-albedo feedback could still push the GrIS beyond a threshold of irreversible demise (Fyke et al., 2018). Although we have observations of atmospheric temperature, they span only the past few decades and represent conditions cooler than those predicted for the future. As a result, contemporary data provide limited constraints on the long-term GrIS response to atmosphere and ocean forcing (Box et al., 2009; Jensen, 2025; Nowicki et al., 2016).

Reconstructing temperature and atmospheric circulation near the margins of the GrIS during past periods of reduced ice sheet size can highlight mechanisms influencing GrIS change today and provide constraints on Greenland Ice Sheet climate sensitivity. Yet, the modern GrIS covers sediment archives deposited during such periods, and many others that may have once existed along the fringes of Greenland were eroded by subsequent glaciations. Here we present new lipid biomarker data from subglacial sediments at Camp Century that constrain past temperature and atmospheric circulation during Marine Isotope Stage (MIS) 11 in northwestern Greenland and evaluate these results in the context of existing marine, ice-core, and terrestrial paleoclimate records.

1.1. Interglacial Climate in Greenland

Climate on Greenland is intimately linked with global heat transport, as Greenland lies between the Labrador Sea and the Nordic Seas, two areas of North Atlantic Deep Water formation (Bullister et al., 2013). The North Atlantic Ocean was relatively warm during the Pliocene (Lawrence et al., 2009). Cooling at the Plio-Pleistocene transition, which manifested during both interglacial and glacial periods at high latitudes, caused Northern Hemisphere ice-sheet growth and altered the global carbon cycle (Herbert et al., 2010; Lawrence et al., 2010). During this interval, tropical and high-latitude temperature became phase-coupled, with synchronous glacial–interglacial changes but differing amplitudes between regions (Herbert et al., 2010; Lawrence et al., 2010). Through the Pleistocene, glacial periods became increasingly cold, whereas temperature between interglacial periods were relatively stable within each region (Herbert et al., 2010; Lawrence et al., 2010). In the North Atlantic region, marine sediment records indicate that mid- to late-Pleistocene interglacial periods exhibited some temperature variability: MIS 9 and 5 were up to ~1 to 2°C warmer than the Holocene, MIS 11 had similar temperature to the Holocene but was much longer, and MIS 7 and 13 were approximately 1°C cooler than the Holocene (Cluett et al., 2021; de Vernal and Hillaire-Marcel, 2008; Irvalı et al., 2020). This contrasts with the eastern Arctic, where lake sediment records indicate 'super interglacial', i.e., extreme, warmth during MIS 11, with similar timing to warmth in the Southern Ocean and Antarctica (Melles et al., 2012).

The highest-resolution climate time series for Greenland are derived from ice cores, some of which span both MIS 1 (the Holocene) and parts of MIS 5 (the Last Interglacial, LIG). These time series suggest that mean annual temperature was 2 to 3°C warmer than modern during peak Holocene warmth (Kobashi et al., 2017; Martin et al., 2024) and 8 ± 4°C warmer during peak LIG warmth (Dahl-Jensen et al., 2013). Yet these ice-core time series are annual averages for high elevation and likely do not closely reflect summer temperature at the ice sheet margins, which governs ablation and in turn impacts ice-sheet mass balance.

A reanalysis product using spatial and seasonal information from a climate model and temporal information from ice-core proxy time series found that middle Holocene Greenland-wide summers were 3.6 ± 0.4°C higher than present (Buizert et al., 2018). Peak Holocene summer temperature around the ice-sheet margins, inferred from biomarkers and insect fossils in lacustrine sediment archives, were 2 to 9°C higher than present from 11.7 to 5.0 ka, with some evidence for greater warming in northern Greenland compared to southern Greenland (Acharya et al., 2026; Axford et al., 2021; Axford et al., 2013; Axford et al., 2017; Axford et al., 2019; Briner et al., 2016; Cluett et al., 2023; McFarlin et al., 2018; Schneider et al., 2024; Thomas et al., 2018). Scattered sediment sections and one extant lake contain pre-Holocene interglacial material with fossils that suggest LIG July temperature was 4.5 to 9.5°C higher than present (Bennike and Böcher, 1992, 1994; Brodersen and Bennike, 2003; Hedenäs, 1994; Hedenäs and Bennike, 2003; McFarlin et al., 2018) and Plio-Pleistocene summer temperatures 6.5 to 8.5°C higher than present (Atti et al., 2024; Bennike, 1990; Bennike et al., 2010; Bennike et al., 2002; Bennike et al., 2023).

The GrIS is additionally sensitive to moisture supply. Ice-sheet model sensitivity tests suggest that the middle Holocene likely experienced greater winter snowfall, which aligns with some proxy evidence interpreted to indicate greater snowfall (Downs et al., 2020; Thomas et al., 2016; Thomas et al., 2020). During the middle Holocene, Greenland also experienced more locally-sourced summer precipitation (Balascio et al., 2013; Thomas et al., 2020) and may have had drier summers compared to present (Aebly and Fritz, 2009; Anderson and Leng, 2004). Therefore, there is evidence that from 11.7 to 5.0 ka, summers around the terrestrial margins of Greenland were warmer than present, accompanied by changes in precipitation seasonality, including greater winter snowfall and drier summers.

Together, these records demonstrate moderate to pronounced warmth in Greenland during interglacial periods, yet significant uncertainties remain. Proxies differ in their seasonal sensitivity, variously capturing peak summer conditions (i.e., July temperature), temperature of the months above freezing, or annual mean temperature (Bennike, 1990; Francis et al., 2006; Otiniano et al., 2024; Raberg et al., 2021). These differences complicate direct inter-proxy comparisons of inferred temperature magnitudes. In addition, the impact of polar amplification, which is the phenomenon whereby temperature changes more rapidly at high latitudes compared to low latitudes due to positive feedbacks, including the sea ice-albedo feedback (Bekryaev et al., 2010; Miller et al., 2010), has not been systematically assessed across available time series. Finally, climate during pre-Holocene interglacial periods, including the LIG, MIS 11, and older Plio-Pleistocene warm intervals, remains poorly constrained due to sparse records, limiting our ability to evaluate the duration, magnitude, and spatial extent of Greenland climate during periods when the GrIS was smaller than present.

1.2. Constraints on Greenland Ice Sheet Extent during Warm Periods

Understanding the implications of past warmth for the GrIS requires knowledge of past GrIS extent. Northern Hemisphere ice sheets grew large enough to deliver significant ice-rafted debris to the surrounding oceans at 2.7 Million years (Ma) (Jansen et al., 2000; Larsen et al., 1994; Raymo et al., 1987; Raymo et al., 1989; Shackleton et al., 1984; St. John and Krissek, 2002). The most direct evidence that the GrIS was likely absent one or more times during the Quaternary comes from cosmogenic nuclide measurements in bedrock beneath the GISP2 ice core, which suggests this site must have been glaciated for at least 820 kyr during the past 1.1 Ma (Schaefer et al., 2016). Continuous time series from marine sediment archives suggest that the GrIS persisted through mid- to late-Pleistocene interglacial periods (Hatfield et al., 2016; Reyes et al., 2014). The southern dome of the GrIS was likely smaller during the prolonged but mild MIS11, but appears to have persisted through brief, warmer interglacials (MIS9, MIS5), perhaps because their warm intervals were of insufficient duration to cause substantial retreat (Cluett and Thomas, 2021; de Vernal and Hillaire-Marcel, 2008; Irvalı et al., 2020).

The minimum GrIS extent during the Middle Holocene has been constrained using proglacial-threshold lakes and reworked marine shells deposited in moraines (Briner et al., 2010; Weidick and Bennike, 2007). This evidence suggests that the timing and size of the GrIS minimum Holocene extent varied around the ice sheet but was generally only minimally reduced in size relative to present (Briner and Bennike, 2025; Briner et al., 2014; Cronauer et al., 2016; Larsen et al., 2015; Tabone et al., 2024). The southwestern portion of the GrIS was likely the farthest behind its modern extent during the middle Holocene (Lecavalier et al., 2014), but more constraints from other regions are required to verify this assessment.

1.3. Gaps in Understanding Pre-Holocene Climate and Ice Sheet Response

The most detailed understanding of both climate and ice sheet extent in Greenland for a previous warm period is for the early and middle Holocene, a period with moderate warmth and moderate, albeit incompletely known, ice-sheet retreat. The greatest number of constraints of pre-Holocene ice-sheet size are from the more widely studied southern region of Greenland. Due to spatial heterogeneity, it is critical to quantify the ice-sheet response in northern Greenland to a range of interglacial conditions, both warmer and longer than the Holocene. It is also critical to quantify climate during pre-Holocene interglacials and assess the spatial expression and mechanisms influencing interglacial warmth. Sub-ice sedimentary archives offer a means to directly constrain the magnitude and timing of past ice-free periods and contain proxies to reconstruct terrestrial environmental conditions near the ice-sheet margins (Bierman et al., 2024a; Bierman et al., 2024b; Christ et al., 2021; Christ et al., 2023; Collins et al., 2025)

This study constrains temperature and precipitation isotope values during the months above freezing for two periods when the ice sheet was smaller than present as recorded in basal sediments at Camp Century: MIS 11 and the Pliocene or Early Pleistocene (Bierman et al., 2024b). We use lipid biomarkers extracted from sub-ice sediments collected in 1966 (Text S1) (Bierman et al., 2024b; Christ et al., 2021; Collins et al., 2025). The biomarkers are distinctive of plants and bacterial communities that exist in extant ice-free areas and therefore had to have been produced under ice-free conditions. To place our findings in a broader spatial context, we also conduct a meta-analysis of published Greenland interglacial temperature and precipitation isotope values and assess the spatial patterns of warmth and water cycle change. This allows us to assess climate conditions during multiple interglacial periods when the GrIS was smaller than present.

2. Methods

2.1. Sediment Core Collection

The Camp Century sediment core comprises 3.44 m of subglacial sediments recovered at the ice-bed interface beneath the Greenland Ice Sheet in northwestern Greenland (Hansen and Langway, 1966) (77.1667°N, -61.1333°E; Figure 1A). The sediments are divided into five stratigraphic units (Units 1-5) based on sedimentological characteristics (Bierman et al., 2024b; Collins et al., 2025). The upper units (Units 3–5) yield a last exposure age of 416 ± 38 ka, interpreted to correspond to the MIS 11 interglacial, based on luminescence dating (Christ et al., 2023), whereas the lower unit (Unit 1) was buried between the Early Pleistocene (>1.4 Ma; infrared-stimulated luminescence) and the Late Pliocene (<3.2 Ma; $^{26}Al/^{10}Be$) (Christ et al., 2021). Additional details on study setting, core recovery, sample subdivision, and processing are provided in Supplementary Information (Texts S1 and S2.1).

2.2. Lipid Biomarker Extraction and Paleoclimate Reconstructions

We extracted, purified, and analyzed *n*-alkanoic acids (plant waxes) and glycerol dialkyl glycerol tetraethers (GDGTs) from the <64 μm grain size sediment fractions following established protocols (Holtzman et al., 2025; Thomas et al., 2023) (details in text S2 and Bierman et al., 2024b). We used the mean of two high-latitude lacustrine calibrations to infer air temperature of the months above freezing (MAF) from branched GDGTs (brGDGTs) (Otiniano et al., 2024; Raberg et al., 2021). The associated calibration errors are 2.14°C and 1°C (RMSE), respectively, and we propagated calibration uncertainty and analytical error into inferred temperature values (Text S3.1, Equations S1 and S2; Figure S1). We used these calibrations since they were derived from high-latitude Arctic lakes (Text 3.1). We inferred lake water δ^2H values using the C_{22} *n*-alkanoic acid in Units 1 and Units 3 to 5 and an estimated apparent fractionation value for aquatic plants in high-latitude lakes, based on compilations of published studies, of -124 ± 5 ‰ (Dion-Kirschner et al., 2020; Gorbey et al., 2022; Hollister et al., 2022) (Equation S5, Text S3.3). We infer leaf water δ^2H values from the C_{28} *n*-alkanoic acid in all five units using estimated biosynthetic fractionation values for high-latitude terrestrial plants in bioclimate zones similar to northwestern Greenland, also based on literature compilations, of -143 ± 5 ‰ (O'Connor et al., 2020) (Equation S6, Text S3.3).

Because we have independent summer temperature and precipitation δ^2H reconstructions, we can estimate the effects of local condensation temperature on summer precipitation δ^2H values, providing insights into the vapor δ^2H values of the airmasses arriving at the Camp Century site (Holtzman et al., 2025; Thomas et al., 2018) (Text S3.4). We calculated the temperature-dependent equilibrium fractionation factor (Clark and Fritz, 1997; Majoube, 1971) using brGDGT-inferred MAF temperature from the same samples as the leaf wax δ^2H measurements and then used the fractionation factor and inferred summer precipitation δ^2H values to estimate summer vapor δ^2H values in each sample (Equations S8 – S9).

2.3. Modern context: Elevation and lapse-rate corrections for comparison with observational data

To place the Camp Century temperature and precipitation isotope reconstructions in the context of modern climate, we first estimated modern air temperature and precipitation isotope values at the Camp Century site under ice-free conditions. This elevation-corrected, bedrock-equivalent modern baseline allows direct comparison between the reconstructed climate and climate that would be expected at the Camp Century site today in the absence of the GrIS. The lapse-rate correction accounts only for the influence of elevation on temperature and precipitation isotope values and does not attempt to incorporate other processes that would accompany ice-sheet retreat, such as changes in surface albedo, atmospheric circulation, or moisture transport, although by correcting to values at a location near the modern ice-sheet margin, we may inadvertently account for some of these factors. Consequently, the corrected values should be interpreted as a topographically adjusted reference baseline rather than a complete simulation of the local climate under ice-free conditions. The nearest meteorological station with precipitation isotope observations is at Pituffik (Figure 1A) (Hersbach et al., 2020; IAEA/WMO, 2015). We lapse-rate adjusted the Pituffik temperature and precipitation isotope values (at 77 m above sea level, asl) to align with the elevation at which the Camp Century sediments were deposited, a value that we estimated as follows. Although the ice-sheet bed at Camp Century is 530 ± 30 m asl today (Morlighem et al., 2017), the land surface elevation would be 810 ± 60 m asl (280 ± 50 m higher than today) following complete removal of GrIS and full isostatic adjustment of the crust (Paxman et al., 2022). Another possibility is that the GrIS was smaller than present but not entirely absent, leading to the possibility that the full isostatic adjustment yields an elevation that is too high. Alternatively, the GrIS margin was inland of, but close to, the Camp Century site. In this case, a forebulge could have caused the elevation to be tens of meters higher than the full isostatic adjustment value (Brandes et al., 2025). This region in northwestern Greenland was influenced by the forebulges of the more massive Innuitian and Laurentide ice sheets (Caron et al., 2018). Given that crustal rebound begins as the GrIS thins and that local forebulge development could increase elevation above the fully compensated value, we therefore use an elevation of 810 ± 60 m as our best estimate of the exposed land surface, with the uncertainty reflecting plausible deviations from full isostatic adjustment and evolution of crustal elevation during ice-sheet retreat.

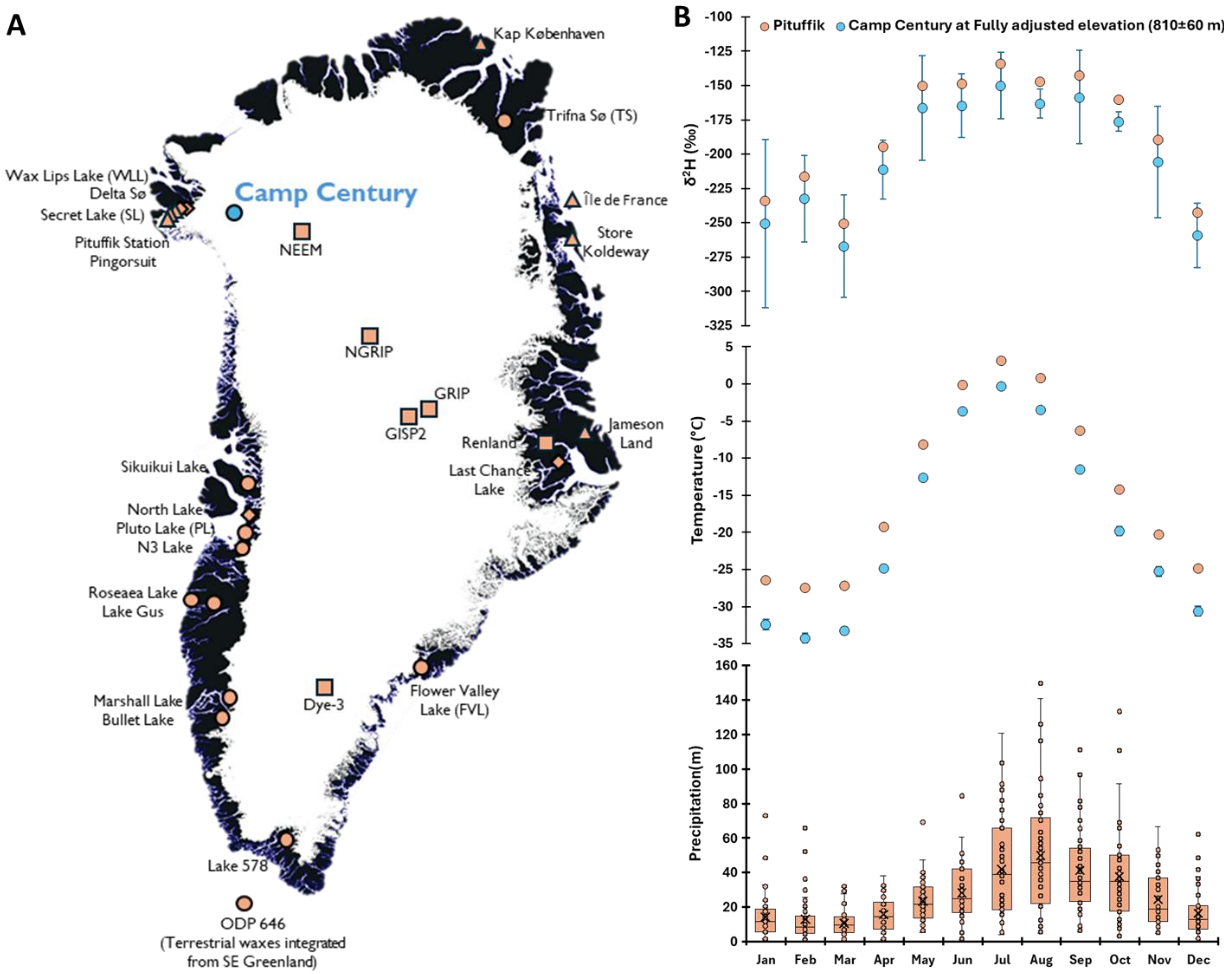

Figure 1. (A) Location (blue circle) of Camp Century (77.1667°N, -61.1333°E), Northwest Greenland and other sites mentioned in text. Orange symbols indicate the locations of sites mentioned in text, including brGDGT and leaf wax (circles), chironomid assemblage (diamonds), ice core (squares), and plant macrofossil (triangles). (B) Pituffik Station (orange) and Camp Century derived via lapse-rate correction (Section 2.3, Text S3.5) (blue) monthly precipitation hydrogen isotope observations (δ^2H) (top, 1966 to 1969 CE) (IAEA/WMO, 2015), air temperature (middle, 1950 to 2000 CE) and precipitation amount (bottom, 1950 to 2000 CE) (Hersbach et al., 2020). δ^2H precipitation and temperature are monthly means; error bars incorporate interannual variability and elevation correction uncertainty (see methods). Precipitation plots illustrate mean (x'es), median and interquartile range (line and box), 5th and 95th percentile (whiskers), and outliers (dots).

We adjust the temperature and precipitation isotope values for the months above freezing at Pituffik from its elevation of 77 m asl to the Camp Century adjusted elevation of 810 m asl, incorporating 60 m of uncertainty into all calculations. We apply lapse rates established for low-elevation, high-latitude sites of ~-5 ± 1°C/km for summer months (Fausto et al., 2009) and -46 ± 8 ‰ δ^2H/km (Koerner and Russell, 1979) (Equations S10 and S11). The 810 ± 60 m adjustment therefore equates to -4°C and -37 ‰, with elevation-related uncertainties of 1°C and 3 ‰. We report a mean-elevation adjusted temperature and precipitation anomaly relative to the late 20th century for each unit, and fully propagate uncertainties, including variance among Camp Century samples in each unit, interannual variance in modern observations, and uncertainties in analyses, lapse-rate, and elevation (Texts S3.1, 3.3, and 3.6).

2.4. Meta-analysis of published Greenland paleoclimate time series

We compiled published Greenland paleoclimate time series for comparison with the Camp Century data, including eight brGDGT, seven ice-core, five chironomid, and six macrofossil records for temperature, and six lake, one marine, and seven ice-core records for precipitation isotope reconstructions. For consistency, we determined the value of each time series relative to the same anomaly period, the late 20th century (Table S1 and S2). Herein, the anomaly period refers to observations from 1950–2000 CE, obtained from ERA5 via Climate Reanalyzer (Hersbach et al., 2020) except for ice-core sites, where modern temperature estimates were taken directly from datasets reported in the original ice-core studies (Buizert et al., 2018; Kobashi et al., 2017). We define 1950–2000 CE as our modern baseline, and refer to this period as “modern” throughout the rest of the text, as it represents a period with robust observational coverage and aligns with the sampling period for precipitation isotope observations (IAEA/WMO, 2015).

These temperature data were used to identify months with mean temperatures above freezing at each study site. Modern precipitation isotope values were extracted from the Online Isotopes in Precipitation Calculator (OIPC), which provides globally calibrated long-term mean isotope fields based on observational data and spatial interpolation (Bowen, 2017; Bowen et al., 2005; IAEA/WMO, 2015). For each site, we calculated the mean modern precipitation isotope value for the months above freezing to allow direct comparison with proxy-derived precipitation isotope values for the months above freezing.

The biomarkers in the Camp Century samples likely integrate environmental signals over timescales of centuries to a few millennia, although the exact temporal resolution is not precisely constrained and may vary between samples. Moreover, the Camp Century stratigraphy likely represents discontinuous preservation of interglacial conditions and may not capture full interglacial means, nor do the samples necessarily capture peak interglacial conditions. To enable comparison with other proxy data, we therefore calculated millennial-scale mean values of published paleoclimate time series that approximate peak warm conditions in each time series. To determine peak Holocene temperature, we calculated the mean of the warmest two millennia between 11.7 and 5.0 ka in each dataset. For brGDGT time series, we used the same proxy-to-temperature calibration approach as for the Camp Century samples (section 2.2 and text S3.1). For chironomid time series, we used the chironomid-July air temperature calibration of Francis et al. (2006), as that was consistently reported by all publications. For precipitation isotope time series, since some datasets do not have independent temperature constraints, we calculated the mean values for 8 to 5 ka, an interval that coincides with peak Holocene warmth on Greenland (Axford et al., 2021; Briner et al., 2016). We used the same plant wax fractionation factor approach to calculate lake and leaf water isotope values for all plant wax time series. Finally, we quantified uncertainties by propagating both the variability within each time series and the errors associated with calibrations. This approach isolates conditions during peak warmth in each time series for comparison with the Camp Century results. For some time series, we know that this interval of peak warmth represents the maximum temperature for a given interglacial period, whereas for other time series that do not necessarily span an entire interglacial period, including Camp Century, the samples provide a minimum estimate of peak warmth.

To compare reconstructions of Greenland temperature based on different proxies, we must understand the seasonal bias of each proxy. brGDGTs reflect MAF temperature, whereas chironomids and plant macrofossils primarily reflect peak summer (July) air temperature (Bennike, 1990; Francis et al., 2006; Otiniano et al., 2024; Raberg et al., 2021). Analysis of modern seasonal temperature relationships at Pituffik Station using ERA5 reanalysis data (Hersbach et al., 2020) shows that although July and MAF air temperatures are strongly and linearly correlated, MAF increases more slowly than July temperature (Figure S2). ERA5 provides a spatially and temporally continuous estimate of modern climatology by assimilating available meteorological observations (Hersbach et al., 2020). While uncertainties remain in data-sparse regions, ERA5 estimates near Pituffik are better constrained by the availability of long-term meteorological observations compared with the GrIS interior (Chen et al., 2026; Zhang et al., 2021).July temperature captures peak summer warmth, while MAF temperature incorporates all months with mean temperature above 0°C, including cooler shoulder-season months, and thus responds more weakly to the same forcing than July temperature. Therefore, chironomid or macrofossil-inferred July temperature anomalies of 7.0°C would be recorded by brGDGTs as a 4.5°C MAF temperature anomaly, assuming the modern relationship is constant through geological time. This is likely a poor assumption, since the length of the MAF season changes with climate, likely causing the MAF-July temperature relationship to change. We therefore do not convert from one seasonal value to another but note that the seasonal biases in proxies cause brGDGT temperature anomalies to be smaller than chironomid or macrofossil anomalies, even under the same climate conditions.

There are a few locations in Greenland with both precipitation isotope and temperature reconstructions (Acharya et al., 2026; Grootes and Stuiver, 1999; Kobashi et al., 2017; Thomas et al., 2020). To compare vapor isotope values at these locations with those reconstructed at Camp Century, we used the same approach applied to the Camp Century data for both the modern and Holocene observations, except for ice core time series, where we applied the fractionation factor for temperatures below freezing (Ellehoj et al., 2013). The isotope time series at Flower Valley and Secret lakes (Balascio et al., 2013; Lasher et al., 2017) do not have independent temperature time series from the same lake, so we used inferred temperature from nearby sites (Text S3.4).

Once we have both the value for the late 20th century anomaly period and the mean value for the published paleoclimate time series, we calculate anomaly values as at Camp Century by calculating the difference between the Holocene, LIG, or Plio-Pleistocene mean values and the late 20th century value. We incorporated uncertainties from both the reconstructed time series and the modern reference dataset (Text S3.7, Table S1 and S2). The anomaly values presented here may differ from those reported in the original studies, as we use ERA5 temperature data from 1950 to 2000 CE and OIPC stable isotope values as the reference values for all sites, whereas the original studies may have used different time periods or sources for the modern anomaly value.

3. Proxy Systematics and Biomarker Interpretation

The lipid biomarkers preserved in the Camp Century sediments can provide information about past temperature and hydrologic conditions in northwestern Greenland. Interpreting the climatic signals from these biomarkers requires understanding the sources, depositional environments, and seasonal sensitivities influencing each proxy system. These factors control the environmental conditions recorded by each proxy and will allow us to identify the settings under which these biomarkers were produced and preserved. Here we report biomarker results from our samples and use measured distributions, isotope values, and published data from similar modern settings to evaluate the proxy systematics of GDGTs and plant wax *n*-alkanoic acids, including their production environments, seasonal biases, and the climatic variables they reflect. This framework provides the basis for reconstructing the temperature and hydrologic conditions recorded in the Camp Century sub-ice sediments at the time the biomarkers were produced.

3.1. GDGTs

Branched GDGTs are membrane lipids primarily produced by bacteria and are commonly found in soils and lake sediments (Sinninghe Damsté et al., 2000), whereas isoGDGTs are produced mainly by archaea, particularly ammonia-oxidizing Thaumarchaeota in aquatic and marine environments (Sinninghe Damsté et al., 2000). We detected brGDGTS and the isoprenoid GDGTs (isoGDGTs) crenarchaeol (cren) and GDGT-0 (caldarchaeol, cald) in all Camp Century samples. Abundances of the other isoGDGTs (GDGT-1, 2, 3, and crenarchaeol regioisomer) were generally below the detection limit, and the Branched to Isoprenoid Tetraether (BIT) index was >0.97 for all samples. Camp Century brGDGT distributions are most similar to brGDGTs from modern high-latitude lakes, rather than peats or soils (Figure S3 & S4) (De Jonge et al., 2015; De Jonge et al., 2021; De Jonge et al., 2019; Dearing Crampton-Flood et al., 2020; Ding et al., 2018; Dugerdil et al., 2021; Guo et al., 2020; Halffman et al., 2022; Kusch et al., 2019; Martínez-Sosa et al., 2021; Naafs et al., 2017a; Naafs et al., 2017b; Raberg et al., 2024; Raberg et al., 2021; Wang et al., 2020; Zhao et al., 2021) so we infer that the brGDGTs in all units in Camp Century were produced in aquatic settings. Independent classification using the BIGMaC algorithm (Martínez-Sosa et al., 2023) also suggests the Camp Century samples are from a lacustrine depositional environment (Table S3), providing additional evidence for a lacustrine source of brGDGT production across all units.

Although it may seem counterintuitive that glacial sediments are dominated by lake-derived GDGTs, we explain this finding as follows: the modern ice-free landscape in northwestern Greenland is dotted with shallow lakes, in some areas covering more than 80% of the landscape (Walcott-George et al., 2025). It is therefore likely that the organic matter preserved in both the subglacial and proglacial units of the Camp Century sub-ice sediments, which integrate material from across the landscape overridden by the ice sheet, includes organic matter from lakes. The concentration of brGDGTs in modern lake sediments is five-fold higher than that in modern soils (Figure S10) (Guo et al., 2020; Hollister et al., 2022; Martínez-Sosa et al., 2021). Lake-derived brGDGTs would therefore readily dominate the brGDGT distribution in a mixture of soil and lake sediments.

Lacustrine brGDGT production can be influenced by suboxic conditions, which may alter the distribution of high-abundance compounds and bias reconstructed temperatures by several degrees (Harning et al., 2025; Raberg et al., 2025). The cald/cren ratio in all Camp Century samples, however, was <10, indicating likely absence of suboxic conditions. We therefore applied two high-latitude lake-based calibrations (Otiniano et al., 2024; Raberg et al., 2021) (Equations S1 and S2; Figure S1) to estimate MAF air temperatures from Camp Century brGDGTs. These calibrations were selected because they were developed using Arctic Lake datasets, where brGDGT distributions exhibit the strongest sensitivity to mean MAF temperature (Otiniano et al., 2024; Raberg et al., 2021).

3.2. Plant wax δ^2H-inferred precipitation δ^2H and evaporation

We follow the PAGES Iso2k framework (Konecky et al., 2020) to structure our isotope proxy interpretation. We first define the measured proxy material and its inferred source (plant origin, seasonality, and source water for *n*-alkanoic acids), then interpret the controls on plant source-water δ^2H values and finally link these to the climate mechanisms influencing precipitation δ^2H values.

3.2.1. Measured and Inferred Material: The Plant Source, Production Season, and Source Water for *n*-Alkanoic Acid Homologs

Determining the plant source of each plant wax homolog establishes the source-water pool for the plant wax hydrogens. All Camp Century samples contained C_{20} through C_{32} *n*-alkanoic acids, with C_{24}–C_{28} as the dominant chain-lengths, and Carbon Preference Index (CPI) > 2 (Equation S4). The long-chain C_{26} and C_{28} *n*-alkanoic acids contain similar trends in concentration, $\delta^{13}C$ values, and $\delta^{2}H$ values in all five Camp Century units (Figure S6 and S7). Likewise, the mid-chain C_{20} and C_{22} *n*-alkanoic acids exhibited similar trends, which were distinct from the long-chain waxes in Unit 1 and Units 3-5, but similar to the trends in the long-chain waxes in Unit 2.

The diverging concentration and $\delta^{2}H$ trends between the mid- and long-chain waxes in all but Unit 2 in the Camp Century sediments suggest that these homologs come from different sources. In Unit 2, all chain lengths likely come from the same source. The C_{24} and C_{30} *n*-alkanoic acids display varying degrees of similarity with the other homologs. The C_{24} is likely from a mix of sources, and the C_{30} generally had high uncertainties for isotope measurements, due to its low concentration. The $\delta^{13}C$ values for C_{28} in all five Camp Century units overlap with $\delta^{13}C$ values of modern Arctic graminoids and shrubs, indicating a terrestrial source for this homolog (Hollister et al., 2022) (Figure S8). In contrast, the $\delta^{13}C$ values for C_{22} in all five Camp Century units overlaps with $\delta^{13}C$ values of modern Arctic graminoids, shrubs, and aquatic mosses. Coupled with evidence for different sources of C_{22} and C_{28} *n*-alkanoic acid homologs in Units 1 and 3–5, we interpret the C_{22} *n*-alkanoic acid to be derived from aquatic plants and the C_{28} *n*-alkanoic acid to be from terrestrial higher plants. For Unit 2, we interpret all chain lengths to be from a terrestrial source and interpret only the C_{28} *n*-alkanoic acid. We discuss only the C_{22} and C_{28} *n*-alkanoic acids hereafter, due to sufficient abundance and distinct grouping with similar chain lengths.

We therefore interpret plant waxes at Camp Century to be derived from both aquatic and terrestrial plants, whereas brGDGTs at Camp Century appear to be dominated by lacustrine production. This difference likely reflects the distinct sources and production magnitudes of these biomarkers. Modern terrestrial and aquatic plants produce comparable concentration of waxes (Hollister et al., 2022), although terrestrial plants may produce substantially greater concentrations in other environments (Dion-Kirschner et al., 2020). In contrast, brGDGT concentration is five-fold greater in modern lake sediments than soils (Guo et al., 2020; Martínez-Sosa et al., 2021) (Figure S10). This difference in production magnitudes likely explains why the Camp Century brGDGTs appear dominated by lacustrine input, while the plant waxes reflect both environments.

3.2.2. Isotope Interpretation: The Mechanisms Influencing Source Water δ^2H values

Plant wax δ^2H values reflect the isotope value of the source water used by plants, with additional influence from evaporative enrichment of leaf water and biosynthetic fractionation (Sachse et al., 2012). Terrestrial plants use soil water, which primarily reflects summer precipitation δ^2H values, as most moisture inputs and active layer water recharge occur during the summer (Chiasson-Poirier et al., 2020; Gorbey et al., 2022; Harning et al., 2024; Thomas et al., 2020). However, the leaf water is typically more ^2H-enriched than the original source water, as evaporation preferentially removes isotopically lighter water molecules (Sachse et al., 2012). As a result, terrestrial plant waxes reflect summer precipitation δ^2H values plus evaporative ^2H-enrichment. On the other hand, aquatic plant wax δ^2H values reflect lake water δ^2H values as these plants take up water directly from their environment with little leaf water evaporative enrichment (Sachse et al., 2012). In Arctic lakes and streams, wax synthesis is greatest during the brief growing season when lakes are ice-free, so aquatic plant lipids predominantly record summer lake water δ^2H values. In open-basin Arctic lakes, the impact of evaporative enrichment is limited early during the ice-free season when leaf flush occurs (Akers et al., 2024; Cluett and

Thomas, 2020; Gorbey et al., 2022; Tipple et al., 2013). Thus, lake water δ^2H that aquatic plants uptake largely reflects summer precipitation δ^2H values. Lake water δ^2H values may be modified by evaporative enrichment, particularly in hydrologically closed lakes (Akers et al., 2024; Cluett and Thomas, 2020; Harning et al., 2024; Kjellman et al., 2022). Because the hydrologic setting of the environments in which the Camp Century aquatic biomarkers were produced is unknown, evaporative enrichment represents a potential source of uncertainty in interpreting the reconstructed source-water δ^2H values.Accordingly, we interpret C_{22} δ^2H values to reflect summer precipitation δ^2H values and C_{28} δ^2H values to represent summer precipitation δ^2H values with evaporative ^2H-enrichment.

3.2.3. Climate Interpretation: The Mechanisms Influencing Precipitation δ^2H values

Precipitation isotope values integrate information about moisture source, transport history, and local condensation temperature (Dansgaard, 1964; Gimeno et al., 2021). We estimate the impact of local condensation temperature using the independent brGDGT-inferred MAF temperature and derive summer vapor δ^2H values (Section 2.2 and Text S3.4). Changes in vapor δ^2H values can therefore be interpreted to reflect changes in moisture source and transport history, without the effects of local condensation temperature. Relatively ^2H-enriched vapor tends to indicate shorter atmospheric moisture residence time, or more proximal transport pathways, while ^2H-depleted vapor occurs with longer atmospheric moisture residence time, due to more distal sources and greater distillation along the transport path (Cluett et al., 2021; Gat, 1996; Nusbaumer et al., 2017).

We interpret ^2H- and ^{18}O-enriched water vapor on Greenland to indicate proportionally more local- than remote-sourced moisture. Roughly 20% of modern summer moisture to Pittuffik is from land north of 60°N in North America, and another 10% from nearby marine sources, Baffin Bay and the Canadian Arctic Archipelago (Cluett et al., 2021). Moisture evapotranspired from these sources has a relatively short travel distance to northwestern Greenland, meaning the isotope value of moisture arriving at Pituffik from these sources is ^{2}H-enriched relative to the remaining 70% of moisture (Cluett et al., 2021; Gimeno et al., 2021). The remaining modern summer moisture to Pituffik is from remote sources in the Atlantic and Pacific Oceans and low-latitude landmasses, which deliver relatively ^{2}H-depleted moisture due to long transport times (Cluett et al., 2021). An increase in the proportion of locally-derived moisture to Greenland would cause vapor and resulting precipitation to be ^{2}H-enriched relative to modern (Cluett et al., 2021).

4. Results

4.1. Age, source, and inferred climate from molecular fossils in the Camp Century sedimentary units

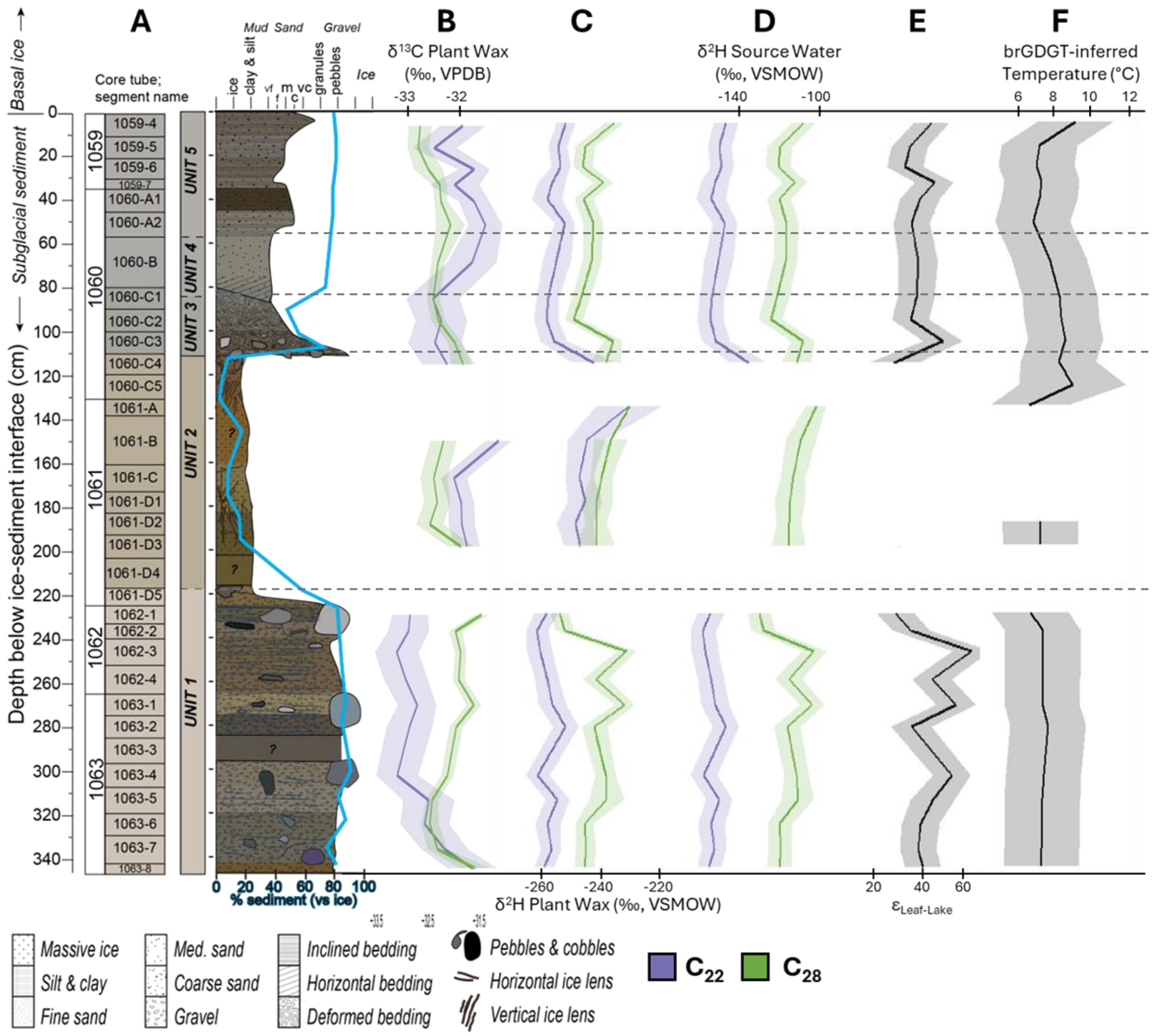

Figure 2. Biomarker data from Camp Century, Northwest Greenland. (A) Stratigraphic units and core log; blue line: percentage of sediment with respect to ice content (Bierman et al., 2024b). (B) $\delta^{13}C$ of C_{22} and C_{28} *n*-alkanoic acids from Camp Century; (C) $\delta^{2}H$ of C_{22} and C_{28} *n*-alkanoic acids from Camp Century. (D) Plant-wax-inferred $\delta^{2}H$ value of lake and leaf water (E) calculated difference between leaf- and lake-water $\delta^{2}H$ values ($\varepsilon_{leaf\text{-}lake}$). (F) brGDT-inferred temperature derived from two high-latitude lacustrine temperature calibrations (Otiniano et al., 2024; Raberg et al., 2021). Shading in B–E incorporates the standard error of the mean associated with the measured $\delta^{2}H$ and $\delta^{13}C$ values, which includes the uncertainty in the peak-size and drift

corrections, the replicate variability, and the methyl group correction. Shading in F represents the propagated standard error, incorporating the standard deviations of the reconstructed temperatures and the RMSEs of both calibrations.

Unit 1 in the Camp Century sub-ice material is characterized by poorly sorted, unstratified sediments with variable grain size and shape, consistent with basal till deposited subglacially as a single massive unit (Bierman et al., 2024b). The biomarkers preserved in this unit likely pre-date deposition, having been incorporated into the till from glacier-entrained soils, lakes, and vegetation present before glaciation. Given that Unit 1 was deposited >1.4 Mya (Christ et al., 2021), these biomarkers likely record climate conditions during the late Pliocene to early Pleistocene. brGDGT-inferred MAF temperatures ranged between 4.3 and 5.0°C (Figure 2F), with mean reconstructed values 4.1 ± 3.4°C above present-day conditions (Figure 3). The δ^2H value of lake water inferred from the C_{22} *n*-alkanoic acid ranged from -158 to -147 ‰, while in Unit 1 the δ^2H value of leaf water inferred from the C_{28} *n*-alkanoic acid ranged from -130 to -103 ‰ in Unit 1 (Figure 2D). Mean summer precipitation δ^2H values were 13 ± 14 ‰ ^2H-enriched relative to modern summer precipitation δ^2H values (Figure 4A). After accounting for the effect of local condensation temperature, summer atmospheric vapor was 19 ± 14 ‰ ^2H-enriched relative to the modern value (Figure 4B). Leaf water was 44 ± 9 ‰ ^2H-enriched relative to lake water (Equation S7, Figure 2E and 5B).

Unit 2 consists predominantly of ice with sparse dispersed sediments. This unit has not been directly dated but is most likely in stratigraphic order relative to Units 1 and 3 and therefore is between early-Pleistocene (Unit 1) and mid-Pleistocene (Unit 3) age. Biomarkers in Unit 2 may have been produced prior to deposition or could be roughly contemporaneous. brGDGT-inferred temperatures ranged from 4.8 to 6.6°C, with greater inter-sample variability than observed in the other units (Figure 2F). Mean MAF temperatures were 4.5 ± 3.1°C above modern conditions (Figure 3). We do not infer mean summer precipitation δ^2H values from Unit 2, as the wax distributions and isotope values indicate only terrestrial plant waxes are present in this Unit. The δ^2H value of leaf water inferred from the C_{28} *n*-alkanoic acid ranged from -116 to -103 ‰ in Unit 2 (Figure 2D), which were slightly ^2H-enriched (5 ± 9 ‰) relative to the leaf water δ^2H values in the other four units but are within uncertainty (Equation S7, Figure 5A).

Units 3 through 5 contain well-sorted, finer-grained sediments with abundant plant macrofossils indicative of an ice-free environment (Bierman et al., 2024b; Collins et al., 2025). Deposited by low- to high-energy flowing water, these units likely represent deposition by summertime streams flowing across a periglacial landscape. The sediments appear to be in stratigraphic order and have been dated to approximately 416,000 ± 38,000 years ago (Christ et al., 2023). Since the depositional environment was likely a subaerial stream surrounded by tundra (Bierman et al., 2024b), the preserved biomarkers were probably produced in nearby tundra and lake landscapes (see Section 3.1: Proxy Systematics) and then transported and deposited at the Camp Century location. brGDGT-inferred MAF temperature ranged from 4.4 to 6.7 in Units 3 to 5. Mean brGDGT-inferred MAF temperature anomalies relative to modern were slightly higher in Unit 3 (5.2 ± 2.4°C) than in Units 4 (4.5 ± 1.8°C) and 5 (4.3 ± 2.9°C), although all are within uncertainty (Figure 3). The δ^2H value of lake water inferred from the C_{22} *n*-alkanoic acid ranged from -154 to -147 ‰ in Units 3 to 5, whereas the δ^2H value of leaf water inferred from the C_{28} *n*-alkanoic acid ranged from -125 to -109 ‰ in Units 3 to 5 (Figure 2D). Mean precipitation δ^2H values for the months above freezing were slightly ^2H-enriched, but within uncertainty of modern precipitation isotope values, with Unit 3 (14 ± 14 ‰) slightly ^2H-depleted relative to Units 4 and 5 (17 ± 14 ‰ and 17 ± 14 ‰, respectively) (Figure 4A). Summer atmospheric vapor δ^2H values were less strongly ^2H-enriched relative to modern vapor in Unit 3 (21 ± 14 ‰) than in Units 4 and 5 (22 ± 14 ‰ and 2 3± 14 ‰, respectively) (Figure 4B). Leaf water was ^2H-enriched relative to lake water, by a similar amount in all three units (~39 ± 9 ‰), similar to those values in unit 1 (Equation S7, Figure 2E and 5B).

4.2. Comparative Analysis of Greenland climate data

4.2.1. brGDGT temperature reconstructions

We compiled and analyzed (Section 2.4) eight published Holocene lacustrine brGDGT time series that form a latitudinal transect spanning southwestern Greenland (Figure 1): Lake 578 (61.080°N), Bullet Lake (63.982°N), Marshall Lake (64.464°N), Rosaea Lake (66.982°N), Lake Gus (67.032°N), Lake N3 (68.836°N), Pluto Lake (69.109°N), and Sikuiui Lake (70.218°N) (Acharya et al., 2026; Cluett et al., 2023; Schneider et al., 2024; Thomas et al., 2018). These publications evaluated potential non-thermal influences on brGDGT distributions, including redox conditions where relevant, and interpreted the time series as primarily reflecting temperature. Using the same approach as we applied to the Camp Century samples, all eight of the Holocene brGDGT-inferred MAF temperatures are around 3 ± 2°C warmer than the modern observation, and about 2 to 3°C cooler than the anomaly reconstructed at Camp Century (Figure 3).

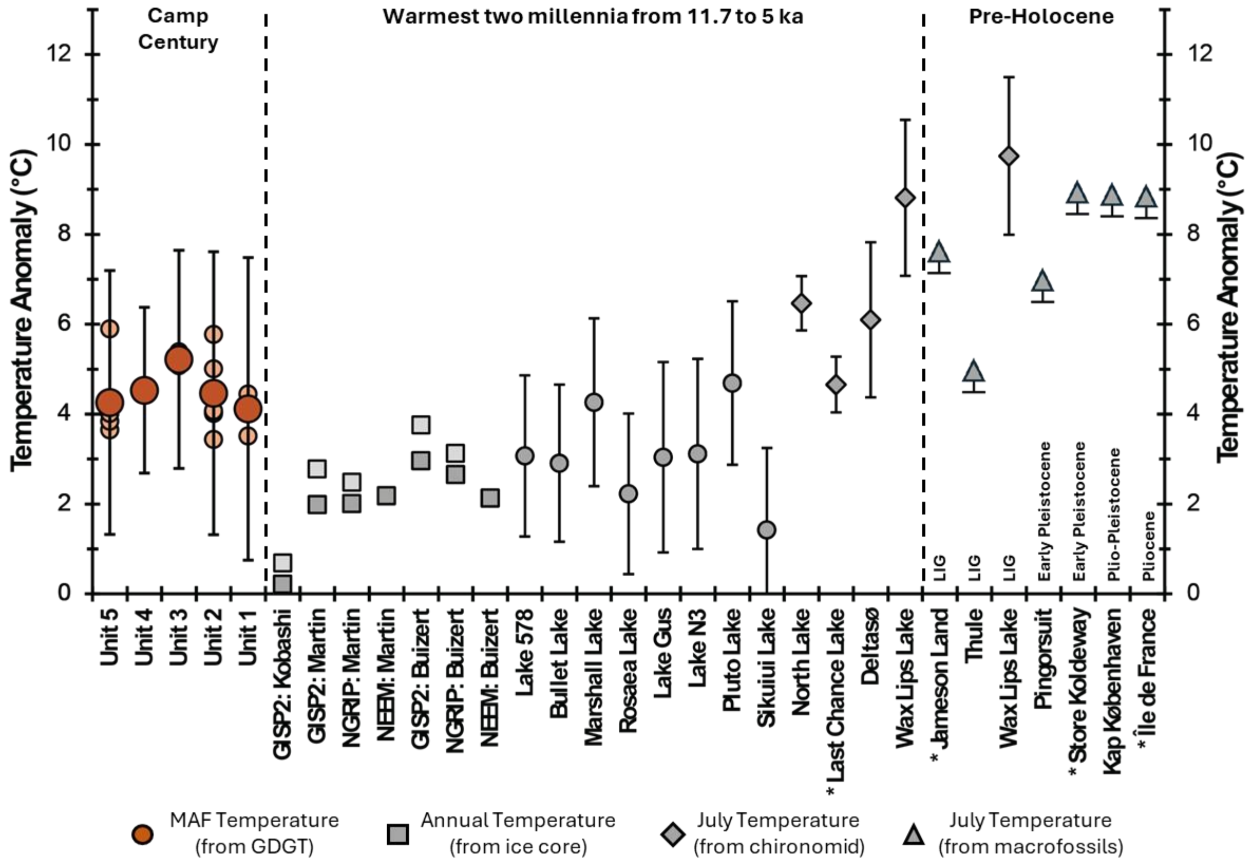

Figure 3. Air temperature anomaly relative to modern values (Table S1) for sites around Greenland. Sites marked with an asterisk (*) are located in eastern Greenland. Left: mean brGDGT-inferred temperature during the months above freezing (MAF) at Camp Century using two high-latitude lacustrine calibrations (Otiniano et al., 2024; Raberg et al., 2021). Light orange circles: individual samples, dark orange circles: mean value for each Unit. Middle: Time series spanning the warmest two millenia from 11.7 to 5.0 ka, each proxy type arranged by latitude from south (left) to north (right). Right: Time series spanning pre-Holocene warm periods (LIG = Last Interglacial), each time period arranged by latitude from south (left) to north (right). Dark gray squares: mean annual air temperature inferred from argon and nitrogen isotopes from ice cores (Kobashi et al., 2017; Martin et al., 2024) and summer (JJA) temperatures inferred from ice core data assimilation (Buizert et al., 2018); Light gray squares: Elevation-corrected inferred temperatures, using elevations from Vinther et al. (2009); Gray circles: brGDGT-inferred MAF air temperature from Greenland lakes (Acharya et al., 2026; Cluett et al., 2023; Schneider et al., 2024; Thomas et al., 2018); gray diamonds: July air temperature inferred from chironomid assemblages using the Francis et al. (2006) calibration (Axford et al., 2013; Axford et al., 2017; Axford et al., 2019; McFarlin et al., 2018); vertical bars and arrow: July temperature inferred from plant macrofossils (Atti et al., 2024; Bennike, 1990; Bennike and Böcher, 1992, 1994; Bennike et al., 2010; Bennike et al., 2002; Bennike et al., 2023; Brodersen and Bennike, 2003; Hedenäs, 1994; Hedenäs and Bennike, 2003). Anomalies are calculated for the relevant seasonality of each proxy. Error bars incorporate propagated uncertainties (see methods). Error bars for ice core data are smaller than the symbol size.

To demonstrate the relative response of these time series independent of calibration choice, we also calculated the MBT′$_{5Me}$ value for the Camp Century units and these eight Holocene time series (Figure S11). MBT′$_{5Me}$ is an index incorporating temperature-sensitive brGDGTs (De Jonge et al., 2014), with a slope of 17.3 to 18.8 index value per °C in Arctic Lake sediments (Otiniano et al., 2024; Zhao et al., 2023). MBT′$_{5Me}$ in Camp Century sedimentary brGDGTs is 0.23 – 0.31 MBT′$_{5Me}$ units higher than the MBT′$_{5Me}$ equivalent of the elevation-adjusted modern temperature at Camp Century (0.79°C) (Figure S11). MBT′$_{5Me}$ values during the warmest two millennia from 11.7 to 5.0 ka at lakes 578 and Gus are ~0.1 MBT′$_{5Me}$ units higher than the uppermost sample in the same cores, whereas at Lake N3, MBT′$_{5Me}$ during this interval are comparable to those of the uppermost sample. Holocene MBT′$_{5Me}$ across all southwestern Greenland lakes is 0.20 – 0.27 MBT′$_{5Me}$ units higher than the MBT′$_{5Me}$ equivalent of the modern MAF temperature at each site.

4.2.2. Chironomid and plant-based temperature reconstructions

There are three Holocene chironomid-inferred July temperature time series that span 69 to 76°N on western Greenland (Figure 1 and 3). These datasets suggest mean July temperature during peak Holocene warmth was around 7.1 ± 2.9°C warmer than the modern observation (Axford et al., 2013; Axford et al., 2019; McFarlin et al., 2018), and approximately 2 to 4°C warmer than the temperature anomaly constructed at Camp Century (Figure 3).

Using the same analytical framework, pre-Holocene chironomid and plant macrofossils reconstructions provided direct comparison with the Camp Century record. Chironomid-inferred July temperature suggests the LIG on northwestern Greenland (76°N) was 9.7 ± 2.9°C warmer than modern July air temperature (McFarlin et al., 2018), and 5 to 6°C higher than the Camp Century MAF temperature anomalies (Figure 3). Plant macrofossil-based estimates provide minimum temperature constraints (and are therefore shown as arrows in Figure 3). During the LIG, Thule (northwestern Greenland) and Jameson Land (eastern Greenland) were at least

4.9°C and 7.5°C warmer than modern July air temperature, and at least 0.3°C and 3°C warmer than Camp Century MAF air temperatures, respectively (Bennike and Böcher, 1992, 1994; Brodersen and Bennike, 2003; Hedenäs, 1994; Hedenäs and Bennike, 2003). Plant macrofossil- and insect-based estimates of Pliocene and Early Pleistocene July temperature at Pingorsuit (northwestern Greenland) and three sites in northeastern and northern Greenland have warmer temperature anomalies compared to those inferred at Camp Century (Atti et al., 2024; Bennike, 1990; Bennike et al., 2010; Bennike et al., 2002; Bennike et al., 2023).

5. Discussion

We infer that the biomarkers in MIS 11 sediments at Camp Century indicate MIS 11 conditions, which is supported by the occurrence of the biomarkers in sediment layers independently interpreted as having been deposited subaerially during the MIS 11 interglacial (Christ et al., 2021). Their presence also requires ice-free conditions at the Camp Century site, which is presently covered by 1387 m of ice. Biomarkers preserved in the Unit 1 and 2 sediments have an unknown age but are likely from sometime in the Pliocene to mid-Pleistocene and were produced when the Camp Century site was ice free. Our data indicate that MAF temperature and precipitation sources during interglacial periods in northwestern Greenland were broadly similar between MIS 11 and the other ice-free intervals recorded in Units 1 and 2. Compared to modern observations, summers were around 4.7°C warmer with a greater proportion of precipitation derived from local sources. These conditions are consistent with local ice-free conditions and the development of active terrestrial and aquatic ecosystems on an ice-free landscape. Comparison of the results with other Greenland paleoclimate records contributes to our understanding on the magnitude and spatial pattern of interglacial warmth across the ice sheet.

5.1. Northwestern Greenland climate: spatial and temporal comparison

5.1.1. Temperature

According to our brGDGT-based reconstruction, the MIS 11 sediments (Units 3-5) indicate that the temperature of the months above freezing in northwestern Greenland was higher than modern (Figure 3). To assess the magnitude of this warming in a broader context, we compare the Camp Century temperatures with other Greenland paleotemperature reconstructions that we compiled from multiple archives. We examine temperature estimates that are not based on water isotopes, as those can be additionally influenced by changes in the hydrological cycle (section 3.2.3.).

Camp Century brGDGT-derived temperatures are similar to or slightly higher than Holocene brGDGT-inferred temperature for southwestern Greenland, consistent with the slightly elevated MBT'_{5Me} values observed in the Camp Century sediments. The slightly higher temperature anomaly during past interglacials at Camp Century compared to the Holocene time series in southwestern Greenland may partly reflect polar amplification, rather than a similar magnitude of warming during the mid- and early Pleistocene and the Holocene. Comparison of Holocene temperature time series derived from the same proxies allows evaluation of polar amplification while minimizing proxy-specific biases. There are no Holocene brGDGT-inferred temperature time series, however, at similar latitudes as the Camp Century site (Figure 1A and 3). The Holocene brGDGT time series spanning southwestern Greenland do not contain evidence for polar amplification of summer temperature, likely due to minimal sea ice cover in the nearby Labrador Sea and Baffin Bay and to a strong West Greenland Current that efficiently transported heat up the southwestern coast of Greenland (Acharya et al., 2026; Cluett et al., 2023; Gibb et al., 2015; Perner et al., 2013; Schneider et al., 2024). Mean-annual temperature inferred at ice-core sites contains evidence for later maximum Holocene temperature at more northern sites, but no difference in the magnitude of warming, even when corrected for elevation and seasonal effects (Figure 3) (Axford et al., 2021; Buizert et al., 2018; Martin et al., 2024). Three Holocene chironomid-inferred July air temperature time series span 69 to 76°N on western Greenland (Figure 1 and 3), and contain equivocal evidence for polar amplification across this portion of Greenland. Two time series from northwestern Greenland have contrasting Holocene anomalies that are similar to and slightly greater than, but within uncertainty of, peak Holocene warmth in central western Greenland (Figure 3) (Axford et al., 2013; Axford et al., 2019; McFarlin et al., 2018).

Collectively, the available brGDGT-, chironomid-, and ice-core-inferred Holocene temperature data contain no strong evidence for polar amplification. If we assume that there was a similar lack of polar amplification across Greenland in pre-Holocene interglacial periods, then the fact that the mean Camp Century brGDGT-inferred MAF temperature anomaly is similar to the warmest two brGDGT-inferred Holocene millennia suggests that MIS11 summers were similar to peak warmth during the Holocene.

Comparing brGDGT-inferred MAF temperature at Camp Century to pre-Holocene temperature estimates elsewhere on Greenland provides a more comprehensive picture of how northwestern Greenland responded to past warmth (Figure 3). It is thought that the LIG period was warmer than modern, yet geological observations and ice-sheet models continue to indicate a wide range of possible ice sheet configurations and retreat during this period (Creel et al., 2026; Dahl-Jensen et al., 2013; Holschuh et al., 2026; Sommers et al., 2021). Temperature reconstructed using water isotopes from the NEEM ice core indicate that northern Greenland experienced temperatures substantially warmer than present during the LIG, with peak anomalies of several degrees above modern (Dahl-Jensen et al., 2013). On the other hand, the early Pleistocene and Pliocene climate and ice-sheet behavior are largely unconstrained. Chironomid and plant macrofossil-based temperature reconstructions indicate temperature anomalies during the LIG and Pliocene-Early Pleistocene that are comparable and slightly higher than those inferred at Camp Century (Atti et al., 2024; Axford et al., 2013; Axford et al., 2019; Bennike, 1990; Bennike and Böcher, 1992, 1994; Bennike et al., 2010; Bennike et al., 2002; Bennike et al., 2023; Brodersen and Bennike, 2003; Hedenäs, 1994; Hedenäs and Bennike, 2003; McFarlin et al., 2018). However, these proxies differ in seasonal signal, as brGDGTs reflect MAF temperatures, whereas chironomid and plant macrofossil assemblages primarily reflect peak summer (particularly July) conditions, which tend to yield larger temperature anomalies. The smaller MAF temperature anomalies in Unit 1 of Camp Century relative to Early Pleistocene plant-based estimates therefore may reflect the difference in seasonal bias rather than reduced regional warmth. Together, these data indicate that the temperature during pre-Holocene interglacial periods in northern Greenland were similar to or slightly warmer than the Holocene.

Uncertainty in the age and origin of biomarkers of Unit 1 of Camp Century and other Early Pleistocene and Pliocene records on Greenland complicates direct comparison. It is possible that these samples were each deposited during a different interglacial or pre-glacial period within the Plio-Pleistocene, each characterized by distinct climatic conditions. The observed differences may reflect variability between separate interglacials rather than inconsistencies among records of the same age. Even so, one key takeaway is that all proxies at all sites suggest temperatures higher than those of the late 20th century.

5.1.2. Water cycle

When the biomarkers in the Camp Century sediments were produced during MIS 11, the Camp Century site had to have been ice-free (i.e., not covered by the GrIS, see section 3.2.1.), meaning there was at least 100 km more land between the west coast of Greenland and the ice-free Camp Century site. This ice-free land not only experienced temperatures above freezing

(Figure 2F), but also supported plant biomass, as indicated by the presence of plants in the Camp Century sediments (Christ et al., 2021). Reduced snow and ice cover and greater plant biomass on Greenland and in high-latitude North America during Pleistocene interglacial periods would result in increased summer terrestrial evapotranspiration, which would cause a greater proportion of local moisture in northwestern Greenland.

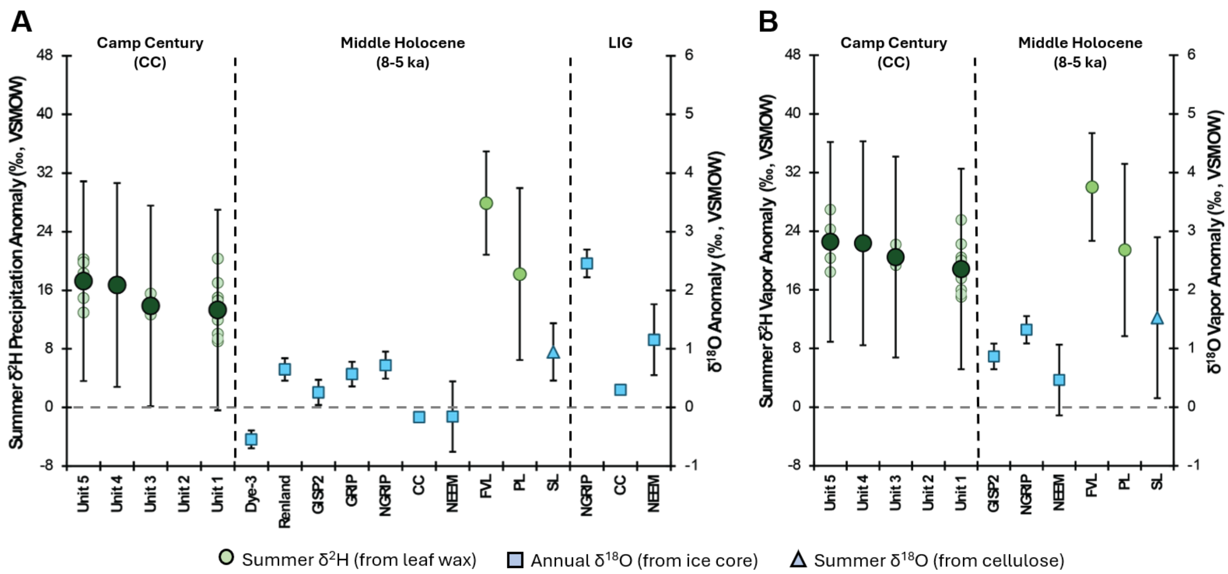

Figure 4. Water isotope anomaly relative to modern values (Table S2) for sites around Greenland. (A) Precipitation δ^2H anomaly (Bowen, 2017; Bowen et al., 2005; IAEA/WMO, 2015). Left: MAF precipitation δ^2H anomalies at Camp Century. Light green circles: individual samples, dark green circles: mean value for each unit. Middle: Middle Holocene (8 to 5 ka). Right: Last interglacial (LIG). (B) Summer vapor δ^2H or $\delta^{18}O$ anomalies derived using the local condensation temperature and precipitation isotope values for both modern (anomaly period) and reconstructed precipitation isotope values (Clark and Fritz, 1997; Ellehoj et al., 2013; Majoube, 1971), using independent temperature reconstructions from the same or nearby archives (Acharya et al., 2026; Axford et al., 2017; Axford et al., 2019; Martin et al., 2024). Blue squares: mean annual precipitation $\delta^{18}O$ from ice cores (Andersen et al., 2004; Dahl-Jensen et al., 2013; Dansgaard et al., 1969; Dansgaard et al., 1982; Grootes and Stuiver, 1997; Johnsen et al., 1997; Schüpbach et al., 2018; Stuiver and Grootes, 2000; Vinther et al., 2009); Green circles: summer precipitation δ^2H inferred from leaf waxes (Balascio et al., 2013; Thomas et al., 2020); Blue triangle: summer precipitation $\delta^{18}O$ inferred from cellulose (Lasher et al., 2017). Error bars incorporate propagated uncertainties (see methods).

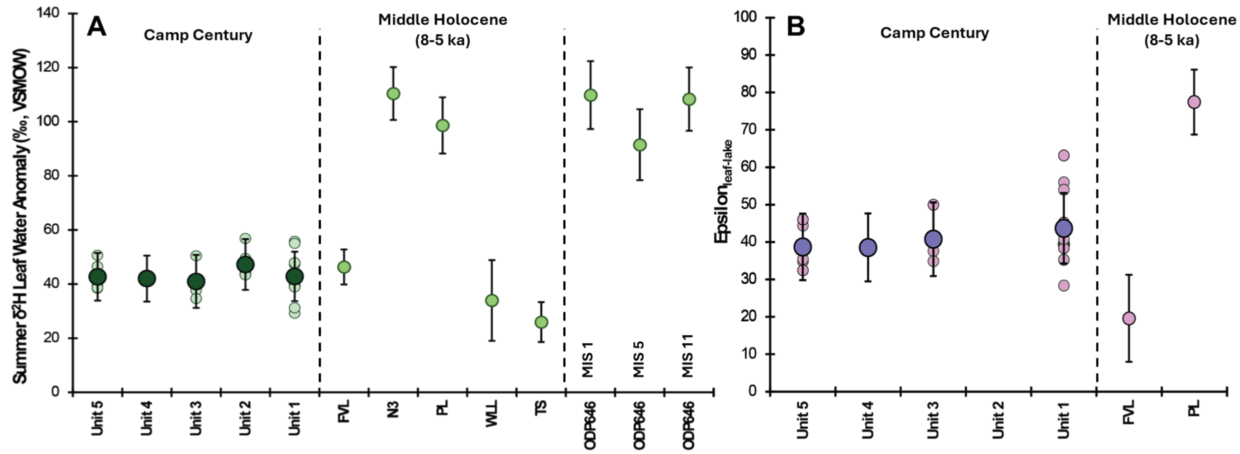

Figure 5. (A) Summer leaf water δ^2H anomaly, which reflects precipitation and evaporation, relative to mean modern summer δ^2H precipitation (Table S2) for sites around Greenland (Bowen, 2017; Bowen et al., 2005; IAEA/WMO, 2015). Left: summer leaf water δ^2H anomaly at Camp Century. Light green circles: individual samples, dark green circles: mean value for each unit. Middle: summer leaf water δ^2H anomalies for Greenland lake records spanning the middle Holocene (8 to 5 ka) (Balascio et al., 2013; McFarlin et al., 2023; Thomas et al., 2020). Right: summer leaf water δ^2H anomalies from SE Greenland records spanning Marine Isotope Stage (MIS) 1, 5 and 11 (Cluett and Thomas, 2021). (B) Left: Calculated isotope differences between inferred leaf water and lake water δ^2H in Camp Century compared to middle Holocene lake time series (right) (Balascio et al., 2013; Thomas et al., 2020). Pink circles: individual samples, violet circles, mean value for each unit. Error bars incorporate propagated uncertainties (see methods).

Our reconstructed summer water vapor isotope values at Camp Century were similar across all units, which have a mean value of 21 ± 19 ‰ ^2H-enriched relative to modern summer water vapor (Figure 4B). This is a larger anomaly than a Holocene $\delta^{18}O$ water vapor anomaly of 1.5 ± 1.4 ‰ (12 ± 11 ‰ when converted to δ^2H values using the Global Meteoric Water Line (GMWL)) at Secret Lake, near Pituffik, Greenland (Figure 4B) (Axford et al., 2019; Dansgaard, 1964; Lasher et al., 2017). We interpret this greater enrichment to reflect an increased contribution of locally derived moisture resulting from enhanced terrestrial evapotranspiration associated with more extensive ice-free vegetation. This suggests that in northwestern Greenland, summer vapor during MIS 11 (and during the periods recorded by Units 1 and 2) was more strongly influenced by local moisture sources than during the Holocene.

Holocene δ^{2}H vapor anomalies at Flower Valley Lake in southeastern Greenland and Pluto Lake in southwestern Greenland are 30 ± 7 ‰ and 21 ± 12 ‰, respectively (Figure 4B) (Balascio et al., 2013; Thomas et al., 2020), indicating that southern Greenland experienced a comparable or slightly greater influence of locally derived moisture sources during the Holocene than did northwestern Greenland. Today, southwestern Greenland receives similar proportions of local and remote moisture as northwestern Greenland (Cluett et al., 2021), suggesting that these regional differences in moisture sourcing were likely amplified under warmer Holocene conditions. The high δ^{2}H values at the southern Greenland sites likely reflect greater evaporation from local seas and transpiration from terrestrial biomass during peak Holocene warmth, which would have contributed more ^{2}H-enriched moisture to vapor (Cluett et al., 2021). In contrast, the relatively small Holocene δ^{18}O anomalies at ice-core sites relative to Camp Century (Figure 4B) likely reflect differences in the seasonal sensitivity of the proxy archives. Ice core δ^{18}O values integrate annual precipitation, but that is weighted by the seasonality of snowfall, which can vary though time (Buizert et al., 2018; He et al., 2021; Kobashi et al., 2017; Martin et al., 2024). In contrast, the Camp Century plant wax and lake-based isotope records primarily reflect summer moisture conditions and are therefore more directly influenced by changes in summer moisture sources (Cluett et al., 2021; Nusbaumer et al., 2017; Sodemann et al., 2008).

This result aligns with evidence for both reduced GrIS extent (Reyes et al., 2014) and increased plant biomass in southern Greenland (de Vernal and Hillaire-Marcel, 2008) during MIS11 compared to both the Holocene and modern. Climate model simulations suggest that forest biomes may have expanded significantly northward in North America during MIS 11, replacing areas that were previously dominated by grasslands and tundra (Kleinen et al., 2014). Thus, ^{2}H-enriched vapor at Camp Century during the early and middle Pleistocene was likely due to greater local evapotranspiration, consistent with reduced GrIS extent compared to both modern and to the period of peak Holocene warmth.

5.2. Summary and Climate Takeaway

MIS 11 summer temperature and moisture sources inferred from the Camp Century sediments complement existing terrestrial and marine temperature reconstructions from the North Atlantic Ocean and from terrestrial archives around Greenland. Because the Camp Century samples we analyzed were deposited at a location that is currently covered by 1387 m of ice, but must have been ice-free during their production, these biomarker-inferred temperature and water cycle data provide constraints on the sensitivity of the GrIS to climate forcing.

Based on the presence of, age constraints on, and abundance of biomarkers in the Camp Century sediments, we can infer that the Camp Century site was ice-free at least twice during the Plio/Pleistocene, once prior to the deposition of the till that forms Unit 1, and another time during MIS11 (Christ et al., 2023). The climate inferred from the Camp Century samples may not describe maximum interglacial conditions, as it is possible that portions of MIS11 are not preserved in the Camp Century stratigraphy, due to lack of deposition or subsequent erosion (Christ et al., 2021; Christ et al., 2023; Collins et al., 2025). For similar reasons, other interglacial periods, including MIS5 and early Pleistocene intervals, may have been ice-free at Camp Century but did not leave a sediment record. Nevertheless, the presence of plant fossils (Christ et al., 2021) and vapor isotope evidence for a greater contribution of local moisture to northwestern Greenland corroborates the inference of reduced ice-sheet extent during MIS 11 and an earlier interval.

These results shed new light on MIS 11 climate on Greenland. Similar summer temperature during the two intervals studied suggest interglacial temperature was relatively stable throughout the Plio-Pleistocene, similar to previous findings (Herbert et al., 2010). During MIS 11, southeastern Greenland experienced moderate summer conditions similar to the Holocene, but that lasted on the order of 30,000 years, which in turn caused dramatic retreat of the southern portions of the GrIS (Cluett and Thomas, 2021; de Vernal and Hillaire-Marcel, 2008; Irvalı et al., 2020; Reyes et al., 2014). Available evidence from Camp Century suggests that northwestern Greenland also experienced MIS11 conditions similar to the Holocene. Therefore, like in southern Greenland, ice-sheet recession during MIS11 in northwestern Greenland may also have been caused by prolonged, rather than extreme, warmth. This interpretation is consistent with ice-sheet modeling showing that sustained moderate summer temperature anomalies over ~16,000 years can produce substantial GrIS mass loss (Robinson et al., 2017).

By 2100 CE, the Arctic will experience mean annual surface temperatures 3.0 to 10.6°C higher than 1950-2000 CE (Lee, 2023). The Camp Century brGDGT-inferred MAF temperature is at the low end of this range (Figure 3). Modern warming at high latitudes, however, is more pronounced in winter, which means that MAF temperatures will likely increase less than the predicted annual mean (Donohoe and Battisti, 2013; Dwyer et al., 2012). Cloud and albedo feedbacks, however, substantially increase GrIS sensitivity to warming under CMIP6 scenarios (Mostue et al., 2024). The Camp Century sub-ice sediments provide evidence that, due to sustained but moderate warmth during MIS11, the GrIS was >100 km behind its present margin, plants colonizing the ice-free land. The new temperature and water cycle constraints provided by biomarkers produced and deposited during MIS11 in Camp Century sub-ice sediments suggest that efforts to reduce both the magnitude and the duration of anthropogenic warmth will be important to restraining future GrIS retreat.

Acknowledgements

We thank the Kalaallit on whose territory Camp Century lies. The University at Buffalo operates on the territory of the Seneca Nation, a member of the Haudenosaunee/Six Nations Confederacy. We thank Owen Cowling, Nancy Leon and Jeff Salacup for laboratory assistance. This research was supported by NSF OPP 2114632 and a Fulbright Norway Scholar Award to EKT.

Conflict of Interest

Some authors are members of the editorial board of Climate of the Past for the special issue “The Camp Century ice and sediment core: new science from a 1966 core that touched the base of the Greenland ice sheet (CP/TC inter-journal SI)”. The findings and conclusions in this article are those of the authors and do not necessarily represent the views of their corresponding affiliated organization.

Data Availability Statement

Extracted samples are archived at the University at Buffalo. The raw lipid biomarker data generated and analyzed in this study are publicly available at the NOAA Paleoclimate Database (Aguilar et al., 2025).

References

Acharya, S., Cluett, A. A., Grogan, A. L., Briner, J. P., Castañeda, I. S., and Thomas, E. K.: Holocene temperatures in southwestern Greenland controlled by topography, ice sheet proximity and oceanic conditions, Climate of the Past, 22, 1401-1421, 10.5194/cp-22-1401-2026, 2026.

Aebly, F. A. and Fritz, S. C.: Palaeohydrology of Kangerlussuaq (Søndre Strømfjord), West Greenland during the last ~8000 years, The Holocene, 19, 91-104, 10.1177/0959683608096601, 2009.

Aguilar, J. M. N., Thomas, E. K., Briner, J. P., Christ, A. J., Bierman, P. R., and Castañeda, I. S.: Camp Century Northwestern Greenland, Fatty Acids and GDGTs, Early and Mid-Pleistocene [dataset], 2025.

Akers, P. D., Kopec, B. G., Klein, E. S., Bailey, H., and Welker, J. M.: The Pivotal Role of Evaporation in Lake Water Isotopic Variability Across Space and Time in a High Arctic Periglacial Landscape, Water Resources Research, 60, e2023WR036121, https://doi.org/10.1029/2023WR036121, 2024.

Andersen, K. K., Azuma, N., Barnola, J. M., Bigler, M., Biscaye, P., Caillon, N., Chappellaz, J., Clausen, H. B., Dahl-Jensen, D., Fischer, H., Flückiger, J., Fritzsche, D., Fujii, Y., Goto-Azuma, K., Grønvold, K., Gundestrup, N. S., Hansson, M., Huber, C., Hvidberg, C. S., Johnsen, S. J., Jonsell, U., Jouzel, J., Kipfstuhl, S., Landais, A., Leuenberger, M., Lorrain, R., Masson-Delmotte, V., Miller, H., Motoyama, H., Narita, H., Popp, T., Rasmussen, S. O., Raynaud, D., Rothlisberger, R., Ruth, U., Samyn, D., Schwander, J., Shoji, H., Siggard-Andersen, M. L., Steffensen, J. P., Stocker, T., Sveinbjörnsdóttir, A. E., Svensson, A., Takata, M., Tison, J. L., Thorsteinsson, T., Watanabe, O., Wilhelms, F., White, J. W. C., and North Greenland Ice Core Project, m.: High-resolution record of Northern Hemisphere climate extending into the last interglacial period, Nature, 431, 147-151, 10.1038/nature02805, 2004.

Anderson, N. J. and Leng, M. J.: Increased aridity during the early Holocene in West Greenland inferred from stable isotopes in laminated-lake sediments, Quaternary Science Reviews, 23, 841-849, https://doi.org/10.1016/j.quascirev.2003.06.013, 2004.

Aschwanden, A., Fahnestock, M. A., Truffer, M., Brinkerhoff, D. J., Hock, R., Khroulev, C., Mottram, R., and Khan, S. A.: Contribution of the Greenland Ice Sheet to sea level over the next millennium, Science Advances, 5, eaav9396, doi:10.1126/sciadv.aav9396, 2019.

Atti, S., Bennike, O., and Weckström, K.: Cladocerans and diatoms from an Early Pleistocene interglacial deposit at Pingorsuit, North-West Greenland, Journal of Paleolimnology, 72, 331-341, 10.1007/s10933-024-00333-z, 2024.

Axford, Y., de Vernal, A., and Osterberg, E. C.: Past Warmth and Its Impacts During the Holocene Thermal Maximum in Greenland, Annual Review of Earth and Planetary Sciences, 49, 279-307, https://doi.org/10.1146/annurev-earth-081420-063858, 2021.

Axford, Y., Losee, S., Briner, J. P., Francis, D. R., Langdon, P. G., and Walker, I. R.: Holocene temperature history at the western Greenland Ice Sheet margin reconstructed from lake sediments, Quaternary Science Reviews, 59, 87-100, https://doi.org/10.1016/j.quascirev.2012.10.024, 2013.

Axford, Y., Levy, L. B., Kelly, M. A., Francis, D. R., Hall, B. L., Langdon, P. G., and Lowell, T. V.: Timing and magnitude of early to middle Holocene warming in East Greenland inferred from chironomids, Boreas, 46, 678-687, https://doi.org/10.1111/bor.12247, 2017.

Axford, Y., Lasher, G. E., Kelly, M. A., Osterberg, E. C., Landis, J., Schellinger, G. C., Pfeiffer, A., Thompson, E., and Francis, D. R.: Holocene temperature history of northwest Greenland – With new ice cap constraints and chironomid assemblages from Deltasø, Quaternary Science Reviews, 215, 160-172, https://doi.org/10.1016/j.quascirev.2019.05.011, 2019.

Balascio, N. L., D'Andrea, W. J., Bradley, R. S., and Perren, B. B.: Biogeochemical evidence for hydrologic changes during the Holocene in a lake sediment record from southeast Greenland, The Holocene, 23, 1428-1439, 10.1177/0959683613493938, 2013.

Bekryaev, R. V., Polyakov, I. V., and Alexeev, V. A.: Role of Polar Amplification in Long-Term Surface Air Temperature Variations and Modern Arctic Warming, Journal of Climate, 23, 3888-3906, https://doi.org/10.1175/2010JCLI3297.1, 2010.

Bennike, O.: The Kap København Formation: stratigraphy and palaeobotany of a Plio-Pleistocene sequence in Peary Land, North Greenland, Meddelelser om Grønland. Geoscience, 23, 85 pp., 10.7146/moggeosci.v23i.141978, 1990.

Bennike, O. and Böcher, J.: Early Weichselian interstadial land biotas at Thule, Northwest Greenland, Boreas, 21, 111-118, https://doi.org/10.1111/j.1502-3885.1992.tb00019.x, 1992.

Bennike, O. and Böcher, J.: Land biotas of the last interglacial/glacial cycle on Jameson Land, East Greenland, Boreas, 23, 479-487, https://doi.org/10.1111/j.1502-3885.1994.tb00615.x, 1994.

Bennike, O., Knudsen, K. L., Abrahamsen, N., Böcher, J., Cremer, H., and Wagner, B.: Early Pleistocene sediments on Store Koldewey, northeast Greenland, Boreas, 39, 603-619, https://doi.org/10.1111/j.1502-3885.2010.00147.x, 2010.

Bennike, O., Abrahamsen, N., Bak, M., Israelson, C., Konradi, P., Matthiessen, J., and Witkowski, A.: A multi-proxy study of Pliocene sediments from Île de France, North-East Greenland, Palaeogeography, Palaeoclimatology, Palaeoecology, 186, 1-23, https://doi.org/10.1016/S0031-0182(02)00439-X, 2002.

Bennike, O., Colgan, W., Hedenäs, L., Heiri, O., Lemdahl, G., Wiberg-Larsen, P., Ribeiro, S., Pronzato, R., Manconi, R., and Bjørk, A. A.: An Early Pleistocene interglacial deposit at Pingorsuit, North-West Greenland, Boreas, 52, 27-41, https://doi.org/10.1111/bor.12596, 2023.

Bierman, P. R., Mastro, H. M., Peteet, D. M., Corbett, L. B., Steig, E. J., Halsted, C. T., Caffee, M. M., Hidy, A. J., Balco, G., Bennike, O., and Rock, B.: Plant, insect, and fungi fossils under the center of Greenland's ice sheet are evidence of ice-free times, Proceedings of the National Academy of Sciences, 121, e2407465121, doi:10.1073/pnas.2407465121, 2024a.

Bierman, P. R., Christ, A. J., Collins, C. M., Mastro, H. M., Souza, J., Blard, P. H., Brachfeld, S., Courville, Z. R., Rittenour, T. M., Thomas, E. K., Tison, J. L., and Fripiat, F.: Scientific history, sampling approach, and physical characterization of the Camp Century sub-glacial sediment core, a rare archive from beneath the Greenland Ice Sheet, EGUsphere, 2024, 1-28, 10.5194/egusphere-2023-2922, 2024b.

The Online Isotopes in Precipitation Calculator: http://www.waterisotopes.org, last

Bowen, G. J., Wassenaar, L. I., and Hobson, K. A.: Global application of stable hydrogen and oxygen isotopes to wildlife forensics, Oecologia, 143, 337-348, 10.1007/s00442-004-1813-y, 2005.

Box, J. E., Yang, L., Bromwich, D. H., and Bai, L.-S.: Greenland Ice Sheet Surface Air Temperature Variability: 1840–2007, Journal of Climate, 22, 4029-4049, https://doi.org/10.1175/2009JCLI2816.1, 2009.

Brandes, C., Steffen, H., Steffen, R., Li, T., and Wu, P.: Effects of the Last Quaternary Glacial Forebulge on Vertical Land Movement, Sea-Level Change, and Lithospheric Stresses, Reviews of Geophysics, 63, e2024RG000852, https://doi.org/10.1029/2024RG000852, 2025.

Briner, J. P. and Bennike, O.: An early Neoglacial moraine at Sanddalen, NE Greenland, Bulletin of the Geological Society of Denmark, 74, 219-225, 10.37570/bgsd-2025-74-12, 2025.

Briner, J. P., Kaufman, D. S., Bennike, O., and Kosnik, M. A.: Amino acid ratios in reworked marine bivalve shells constrain Greenland Ice Sheet history during the Holocene, Geology, 42, 75-78, 10.1130/g34843.1, 2014.

Briner, J. P., Stewart, H. A. M., Young, N. E., Philipps, W., and Losee, S.: Using proglacial-threshold lakes to constrain fluctuations of the Jakobshavn Isbræ ice margin, western Greenland, during the Holocene, Quaternary Science Reviews, 29, 3861-3874, https://doi.org/10.1016/j.quascirev.2010.09.005, 2010.

Briner, J. P., McKay, N. P., Axford, Y., Bennike, O., Bradley, R. S., de Vernal, A., Fisher, D., Francus, P., Fréchette, B., Gajewski, K., Jennings, A., Kaufman, D. S., Miller, G., Rouston, C., and Wagner, B.: Holocene climate change in Arctic Canada and Greenland, Quaternary Science Reviews, 147, 340-364, https://doi.org/10.1016/j.quascirev.2016.02.010, 2016.

Brodersen, K. P. and Bennike, O.: Interglacial Chironomidae (Diptera) from Thule, Northwest Greenland: matching modern analogues to fossil assemblages, Boreas, 32, 560-565, https://doi.org/10.1111/j.1502-3885.2003.tb01235.x, 2003.

Buizert, C., Keisling, B. A., Box, J. E., He, F., Carlson, A. E., Sinclair, G., and DeConto, R. M.: Greenland-Wide Seasonal Temperatures During the Last Deglaciation, Geophysical Research Letters, 45, 1905-1914, https://doi.org/10.1002/2017GL075601, 2018.

Bullister, J. L., Rhein, M., and Mauritzen, C.: Chapter 10 - Deepwater Formation, in: International Geophysics, edited by: Siedler, G., Griffies, S. M., Gould, J., and Church, J. A., Academic Press, 227-253, https://doi.org/10.1016/B978-0-12-391851-2.00010-6, 2013.

Callard, S. L., Ó Cofaigh, C., Lloyd, J. M., A. Smith, J., Gebhardt, C. A., Kanzow, T., and Roberts, D. H.: Ocean driven retreat of the Northeast Greenland Ice Stream following the Last Glacial Maximum, Nature Communications, 16, 10961, 10.1038/s41467-025-66671-2, 2025.

Caron, L., Ivins, E. R., Larour, E., Adhikari, S., Nilsson, J., and Blewitt, G.: GIA Model Statistics for GRACE Hydrology, Cryosphere, and Ocean Science, Geophysical Research Letters, 45, 2203-2212, https://doi.org/10.1002/2017GL076644, 2018.

Chen, Z.-M., Zeng, Z.-L., Ding, M.-H., and Wang, Y.-Q.: Comprehensive evaluation of multi-source reanalysis datasets for surface atmospheric parameters over the Greenland Ice Sheet, Advances in Climate Change Research, 17, 48-64, https://doi.org/10.1016/j.accre.2025.10.007, 2026.

Chiasson-Poirier, G., Franssen, J., Lafrenière, M. J., Fortier, D., and Lamoureux, S. F.: Seasonal evolution of active layer thaw depth and hillslope-stream connectivity in a permafrost watershed, Water Resources Research, 56, e2019WR025828, https://doi.org/10.1029/2019WR025828, 2020.

Christ, A. J., Bierman, P. R., Schaefer, J. M., Dahl-Jensen, D., Steffensen, J. P., Corbett, L. B., Peteet, D. M., Thomas, E. K., Steig, E. J., Rittenour, T. M., Tison, J.-L., Blard, P.-H., Perdrial, N., Dethier, D. P., Lini, A., Hidy, A. J., Caffee, M. W., and Southon, J.: A multimillion-year-old record of Greenland vegetation and glacial history preserved in sediment beneath 1.4 km of ice at Camp Century, Proceedings of the National Academy of Sciences, 118, e2021442118, 10.1073/pnas.2021442118, 2021.

Christ, A. J., Rittenour, T. M., Bierman, P. R., Keisling, B. A., Knutz, P. C., Thomsen, T. B., Keulen, N., Fosdick, J. C., Hemming, S. R., Tison, J.-L., Blard, P.-H., Steffensen, J. P., Caffee, M. W., Corbett, L. B., Dahl-Jensen, D., Dethier, D. P., Hidy, A. J., Perdrial, N., Peteet, D. M., Steig, E. J., and Thomas, E. K.: Deglaciation of northwestern Greenland during Marine Isotope Stage 11, Science, 381, 330-335, doi:10.1126/science.ade4248, 2023.

Clark, I. D. and Fritz, P.: Environmental Isotopes in Hydrogeology, 1st, CRC Press, Boca Raton, FL, 10.1201/9781482242911, 1997.

Cluett, A. A. and Thomas, E. K.: Resolving combined influences of inflow and evaporation on western Greenland lake water isotopes to inform paleoclimate inferences, Journal of Paleolimnology, 63, 251-268, 10.1007/s10933-020-00114-4, 2020.

Cluett, A. A. and Thomas, E. K.: Summer warmth of the past six interglacials on Greenland, Proceedings of the National Academy of Sciences, 118, e2022916118, doi:10.1073/pnas.2022916118, 2021.

Cluett, A. A., Thomas, E. K., Evans, S. M., and Keys, P. W.: Seasonal Variations in Moisture Origin Explain Spatial Contrast in Precipitation Isotope Seasonality on Coastal Western Greenland., Journal of Geophysical Research: Biogeosciences, 126, 2021.

Cluett, A. A., Thomas, E. K., McKay, N. P., Cowling, O. C., Castañeda, I. S., and Morrill, C.: Lake Dynamics Modulate the Air Temperature Variability Recorded by Sedimentary Aquatic Biomarkers: A Holocene Case Study From Western Greenland, Journal of Geophysical Research: Biogeosciences, 128, e2022JG007106, https://doi.org/10.1029/2022JG007106, 2023.

Collins, C. M., Perdrial, N., Blard, P. H., Keulen, N., Mahaney, W. C., Mastro, H., Souza, J., Rizzo, D. M., Marrocchi, Y., Knutz, P. C., and Bierman, P. R.: Characterization of the 1966 Camp Century subglacial core: a multiscale analysis, Clim. Past, 21, 1359-1381, 10.5194/cp-21-1359-2025, 2025.

Creel, R. C., Kopp, R. E., Dutton, A., Zhou, Y., Raymo, M. E., Britt, C. J., and DeConto, R. M.: North American ice sheet persistence into past interglacials should inform future projections, Nature Communications, 17, 2280, 10.1038/s41467-026-70032-y, 2026.

Cronauer, S. L., Briner, J. P., Kelley, S. E., Zimmerman, S. R. H., and Morlighem, M.: 10Be dating reveals early-middle Holocene age of the Drygalski Moraines in central West Greenland, Quaternary Science Reviews, 147, 59-68, https://doi.org/10.1016/j.quascirev.2015.08.034, 2016.

Dahl-Jensen, D., Albert, M. R., Aldahan, A., Azuma, N., Balslev-Clausen, D., Baumgartner, M., Berggren, A. M., Bigler, M., Binder, T., Blunier, T., Bourgeois, J. C., Brook, E. J., Buchardt, S. L., Buizert, C., Capron, E., Chappellaz, J., Chung, J., Clausen, H. B., Cvijanovic, I., Davies, S. M., Ditlevsen, P., Eicher, O., Fischer, H., Fisher, D. A., Fleet, L. G., Gfeller, G., Gkinis, V., Gogineni, S., Goto-Azuma, K., Grinsted, A., Gudlaugsdottir, H., Guillevic, M., Hansen, S. B., Hansson, M., Hirabayashi, M., Hong, S., Hur, S. D., Huybrechts, P., Hvidberg, C. S., Iizuka, Y., Jenk, T., Johnsen, S. J., Jones, T. R., Jouzel, J., Karlsson, N. B., Kawamura, K., Keegan, K., Kettner, E., Kipfstuhl, S., Kjær, H. A., Koutnik, M., Kuramoto, T., Köhler, P., Laepple, T., Landais, A., Langen, P. L., Larsen, L. B., Leuenberger, D., Leuenberger, M., Leuschen, C., Li, J., Lipenkov, V., Martinerie, P., Maselli, O. J., Masson-Delmotte, V., McConnell, J. R., Miller, H., Mini, O., Miyamoto, A., Montagnat-Rentier, M., Mulvaney, R., Muscheler, R., Orsi, A. J., Paden, J., Panton, C., Pattyn, F., Petit, J. R., Pol, K., Popp, T., Possnert, G., Prié, F., Prokopiou, M., Quiquet, A., Rasmussen, S. O., Raynaud, D., Ren, J., Reutenauer, C., Ritz, C., Röckmann, T., Rosen, J. L., Rubino, M., Rybak, O., Samyn, D., Sapart, C. J., Schilt, A., Schmidt, A. M. Z., Schwander, J., Schüpbach, S., Seierstad, I., Severinghaus, J. P., Sheldon, S., Simonsen, S. B., Sjolte, J., Solgaard, A. M., Sowers, T., Sperlich, P., Steen-Larsen, H. C., Steffen, K., Steffensen, J. P., Steinhage, D., Stocker, T. F., Stowasser, C., Sturevik, A. S., Sturges, W. T., Sveinbjörnsdottir, A., Svensson, A., Tison, J. L., Uetake, J., Vallelonga, P., van de Wal, R. S. W., van der Wel, G., Vaughn, B. H., Vinther, B., Waddington, E., Wegner, A., Weikusat, I., White, J. W. C., Wilhelms, F., Winstrup, M., Witrant, E., Wolff, E. W., Xiao, C., Zheng, J., and members, N. c.: Eemian interglacial reconstructed from a Greenland folded ice core, Nature, 493, 489-494, 10.1038/nature11789, 2013.

Dansgaard, W.: Stable isotopes in precipitation, Tellus, 16, 436-468, https://doi.org/10.1111/j.2153-3490.1964.tb00181.x, 1964.

Dansgaard, W., Johnsen, S. J., Møller, J., and Langway, C. C.: One Thousand Centuries of Climatic Record from Camp Century on the Greenland Ice Sheet, Science, 166, 377-381, doi:10.1126/science.166.3903.377, 1969.

Dansgaard, W., Clausen, H. B., Gundestrup, N., Hammer, C. U., Johnsen, S. F., Kristinsdottir, P. M., and Reeh, N.: A New Greenland Deep Ice Core, Science, 218, 1273-1277, doi:10.1126/science.218.4579.1273, 1982.

De Jonge, C., Stadnitskaia, A., Fedotov, A., and Sinninghe Damsté, J. S.: Impact of riverine suspended particulate matter on the branched glycerol dialkyl glycerol tetraether composition of lakes: The outflow of the Selenga River in Lake Baikal (Russia), Organic Geochemistry, 83-84, 241-252, https://doi.org/10.1016/j.orggeochem.2015.04.004, 2015.

De Jonge, C., Hopmans, E. C., Zell, C. I., Kim, J.-H., Schouten, S., and Sinninghe Damsté, J. S.: Occurrence and abundance of 6-methyl branched glycerol dialkyl glycerol tetraethers in soils: Implications for palaeoclimate reconstruction, Geochimica et Cosmochimica Acta, 141, 97-112, https://doi.org/10.1016/j.gca.2014.06.013, 2014.

De Jonge, C., Kuramae, E. E., Radujković, D., Weedon, J. T., Janssens, I. A., and Peterse, F.: The influence of soil chemistry on branched tetraether lipids in mid- and high latitude soils: Implications for brGDGT- based paleothermometry, Geochimica et Cosmochimica Acta, 310, 95-112, https://doi.org/10.1016/j.gca.2021.06.037, 2021.

De Jonge, C., Radujković, D., Sigurdsson, B. D., Weedon, J. T., Janssens, I., and Peterse, F.: Lipid biomarker temperature proxy responds to abrupt shift in the bacterial community composition in geothermally heated soils, Organic Geochemistry, 137, 103897, https://doi.org/10.1016/j.orggeochem.2019.07.006, 2019.

de Vernal, A. and Hillaire-Marcel, C.: Natural Variability of Greenland Climate, Vegetation, and Ice Volume During the Past Million Years, Science, 320, 1622-1625, doi:10.1126/science.1153929, 2008.

Dearing Crampton-Flood, E., Tierney, J. E., Peterse, F., Kirkels, F. M. S. A., and Sinninghe Damsté, J. S.: BayMBT: A Bayesian calibration model for branched glycerol dialkyl glycerol tetraethers in soils and peats, Geochimica et Cosmochimica Acta, 268, 142-159, https://doi.org/10.1016/j.gca.2019.09.043, 2020.

Ding, S., Kohlhepp, B., Trumbore, S., Küsel, K., Totsche, K.-U., Pohnert, G., Gleixner, G., and Schwab, V. F.: In situ production of core and intact bacterial and archaeal tetraether lipids in groundwater, Organic Geochemistry, 126, 1-12, https://doi.org/10.1016/j.orggeochem.2018.10.005, 2018.

Dion-Kirschner, H., McFarlin, J. M., Masterson, A. L., Axford, Y., and Osburn, M. R.: Modern constraints on the sources and climate signals recorded by sedimentary plant waxes in west Greenland, Geochimica et Cosmochimica Acta, 286, 336-354, https://doi.org/10.1016/j.gca.2020.07.027, 2020.

Donohoe, A. and Battisti, D. S.: The Seasonal Cycle of Atmospheric Heating and Temperature, Journal of Climate, 26, 4962-4980, https://doi.org/10.1175/JCLI-D-12-00713.1, 2013.

Downs, J., Johnson, J., Briner, J., Young, N., Lesnek, A., and Cuzzone, J.: Western Greenland ice sheet retreat history reveals elevated precipitation during the Holocene thermal maximum, The Cryosphere, 14, 1121-1137, 10.5194/tc-14-1121-2020, 2020.

Dugerdil, L., Ménot, G., Peyron, O., Jouffroy-Bapicot, I., Ansanay-Alex, S., Antheaume, I., Behling, H., Boldgiv, B., Develle, A.-L., Grossi, V., Magail, J., Makou, M., Robles, M., Unkelbach, J., Vannière, B., and Joannin, S.: Late Holocene Mongolian climate and environment reconstructions from brGDGTs, NPPs and pollen transfer functions for Lake Ayrag: Paleoclimate implications for Arid Central Asia, Quaternary Science Reviews, 273, 107235, https://doi.org/10.1016/j.quascirev.2021.107235, 2021.

Dwyer, J. G., Biasutti, M., and Sobel, A. H.: Projected Changes in the Seasonal Cycle of Surface Temperature, Journal of Climate, 25, 6359-6374, https://doi.org/10.1175/JCLI-D-11-00741.1, 2012.

Ellehoj, M. D., Steen-Larsen, H. C., Johnsen, S. J., and Madsen, M. B.: Ice-vapor equilibrium fractionation factor of hydrogen and oxygen isotopes: Experimental investigations and implications for stable water isotope studies, Rapid Communications in Mass Spectrometry, 27, 2149-2158, https://doi.org/10.1002/rcm.6668, 2013.

Fausto, R. S., Ahlstrøm, A. P., Van As, D., Bøggild, C. E., and Johnsen, S. J.: A new present-day temperature parameterization for Greenland, Journal of Glaciology, 55, 95-105, 10.3189/002214309788608985, 2009.

Francis, D. R., Wolfe, A. P., Walker, I. R., and Miller, G. H.: Interglacial and Holocene temperature reconstructions based on midge remains in sediments of two lakes from Baffin Island, Nunavut, Arctic Canada, Palaeogeography, Palaeoclimatology, Palaeoecology, 236, 107-124, https://doi.org/10.1016/j.palaeo.2006.01.005, 2006.

Fyke, J., Sergienko, O., Löfverström, M., Price, S., and Lenaerts, J. T. M.: An Overview of Interactions and Feedbacks Between Ice Sheets and the Earth System, Reviews of Geophysics, 56, 361-408, https://doi.org/10.1029/2018RG000600, 2018.

Gat, J. R.: OXYGEN AND HYDROGEN ISOTOPES IN THE HYDROLOGIC CYCLE, Annual Review of Earth and Planetary Sciences, 24, 225-262, https://doi.org/10.1146/annurev.earth.24.1.225, 1996.

Gibb, O. T., Steinhauer, S., Fréchette, B., de Vernal, A., and Hillaire-Marcel, C.: Diachronous evolution of sea surface conditions in the Labrador Sea and Baffin Bay since the last deglaciation, The Holocene, 25, 1882-1897, 10.1177/0959683615591352, 2015.

Gimeno, L., Eiras-Barca, J., Durán-Quesada, A. M., Dominguez, F., van der Ent, R., Sodemann, H., Sánchez-Murillo, R., Nieto, R., and Kirchner, J. W.: The residence time of water vapour in the atmosphere, Nature Reviews Earth & Environment, 2, 558-569, 10.1038/s43017-021-00181-9, 2021.

Gorbey, D. B., Thomas, E. K., Sauer, P. E., Raynolds, M. K., Miller, G. H., Corcoran, M. C., Cowling, O. C., Crump, S. E., Lovell, K., and Raberg, J. H.: Modern Eastern Canadian Arctic Lake Water Isotopes Exhibit Latitudinal Patterns in Inflow Seasonality and Minimal Evaporative Enrichment, Paleoceanography and Paleoclimatology, 37, e2021PA004384, https://doi.org/10.1029/2021PA004384, 2022.

Grootes, P. M. and Stuiver, M.: Oxygen 18/16 variability in Greenland snow and ice with 10−3- to 105-year time resolution, Journal of Geophysical Research: Oceans, 102, 26455-26470, https://doi.org/10.1029/97JC00880, 1997.

Grootes, P. M. and Stuiver, M.: GISP2 Oxygen Isotope Data (1 year averages), PANGAEA [dataset], 10.1594/PANGAEA.55532, 1999.

Guo, J., Glendell, M., Meersmans, J., Kirkels, F., Middelburg, J. J., and Peterse, F.: Assessing branched tetraether lipids as tracers of soil organic carbon transport through the Carminowe Creek catchment (southwest England), Biogeosciences, 17, 3183-3201, 10.5194/bg-17-3183-2020, 2020.

Guo, X., Zhao, L., Gladstone, R. M., Sun, S., and Moore, J. C.: Simulated retreat of Jakobshavn Isbræ during the 21st century, The Cryosphere, 13, 3139-3153, 10.5194/tc-13-3139-2019, 2019.

Halffman, R., Lembrechts, J., Radujković, D., De Gruyter, J., Nijs, I., and De Jonge, C.: Soil chemistry, temperature and bacterial community composition drive brGDGT distributions along a subarctic elevation gradient, Organic Geochemistry, 163, 104346, https://doi.org/10.1016/j.orggeochem.2021.104346, 2022.

Hansen, B. L. and Langway, C. C.: Deep core drilling in ice and core analysis at Camp Century, Greenland, 1961–66, Antarctic Journal of the United States, 1, 207-208, 1966.

Harning, D. J., Sacco, S., Raberg, J. H., Ardenghi, N., Sepúlveda, J., Shapiro, B., Miller, G. H., and Geirsdóttir, Á.: Both redox potential and climate control molecular proxies in Icelandic Holocene lake sediments, Communications Earth & Environment, 6, 763, 10.1038/s43247-025-02701-7, 2025.

Harning, D. J., Raberg, J. H., McFarlin, J. M., Axford, Y., Florian, C. R., Ólafsdóttir, K. B., Kopf, S., Sepúlveda, J., Miller, G. H., and Geirsdóttir, Á.: Spatiotemporal variation of modern lake, stream, and soil water isotopes in Iceland, Hydrol. Earth Syst. Sci., 28, 4275-4293, 10.5194/hess-28-4275-2024, 2024.

Hatfield, R. G., Reyes, A. V., Stoner, J. S., Carlson, A. E., Beard, B. L., Winsor, K., and Welke, B.: Interglacial responses of the southern Greenland ice sheet over the last 430,000 years determined using particle-size specific magnetic and isotopic tracers, Earth and Planetary Science Letters, 454, 225-236, https://doi.org/10.1016/j.epsl.2016.09.014, 2016.

He, C., Liu, Z., Otto-Bliesner, B. L., Brady, E. C., Zhu, C., Tomas, R., Buizert, C., and Severinghaus, J. P.: Abrupt Heinrich Stadial 1 cooling missing in Greenland oxygen isotopes, Science Advances, 7, eabh1007, doi:10.1126/sciadv.abh1007, 2021.

Hedenäs, L.: Bryophytes from the last interglacial/glacial cycle, Jameson Land, East Greenland, Boreas, 23, 488-494, https://doi.org/10.1111/j.1502-3885.1994.tb00616.x, 1994.

Hedenäs, L. and Bennike, O.: Moss Remains from the Last Interglacial at Thule, NW Greenland, Lindbergia, 28, 52-58, 2003.

Herbert, T. D., Peterson, L. C., Lawrence, K. T., and Liu, Z.: Tropical Ocean Temperatures Over the Past 3.5 Million Years, Science, 328, 1530-1534, doi:10.1126/science.1185435, 2010.

Hersbach, H., Bell, B., Berrisford, P., Hirahara, S., Horányi, A., Muñoz-Sabater, J., Nicolas, J., Peubey, C., Radu, R., Schepers, D., Simmons, A., Soci, C., Abdalla, S., Abellan, X., Balsamo, G., Bechtold, P., Biavati, G., Bidlot, J., Bonavita, M., De Chiara, G., Dahlgren, P., Dee, D., Diamantakis, M., Dragani, R., Flemming, J., Forbes, R., Fuentes, M., Geer, A., Haimberger, L., Healy, S., Hogan, R. J., Hólm, E., Janisková, M., Keeley, S., Laloyaux, P., Lopez, P., Lupu, C., Radnoti, G., de Rosnay, P., Rozum, I., Vamborg, F., Villaume, S., and Thépaut, J.-N.: The ERA5 global reanalysis, Quarterly Journal of the Royal Meteorological Society, 146, 1999-2049, https://doi.org/10.1002/qj.3803, 2020.

Holland, D. M., Thomas, R. H., de Young, B., Ribergaard, M. H., and Lyberth, B.: Acceleration of Jakobshavn Isbræ triggered by warm subsurface ocean waters, Nature Geoscience, 1, 659-664, 10.1038/ngeo316, 2008.

Hollister, K. V., Thomas, E. K., Raynolds, M. K., Bültmann, H., Raberg, J. H., Miller, G. H., and Sepúlveda, J.: Aquatic and Terrestrial Plant Contributions to Sedimentary Plant Waxes in a Modern Arctic Lake Setting, Journal of Geophysical Research: Biogeosciences, 127, e2022JG006903, https://doi.org/10.1029/2022JG006903, 2022.

Holschuh, N., Christianson, K., Dienstfrey, W., Hills, B., Hoffman, A. O., Paden, J., Winter, K., and Zuraw, R.: Entrained debris records regrowth of the Greenland Ice Sheet after the last interglacial, Nature Geoscience, 19, 573-580, 10.1038/s41561-026-01950-1, 2026.

Holtzman, H., Thomas, E. K., Erb, M., Marshall, L., Castañeda, I. S., Kaufman, D., McKay, N. P., and Melles, M.: Early Holocene Atmospheric Circulation Changes Over Northern Europe Based on Isotopic and Biomarker Evidence From Kola Peninsula, Paleoceanography and Paleoclimatology, 40, e2024PA005076, https://doi.org/10.1029/2024PA005076, 2025.

IAEA/WMO: Global Network of Isotopes in Precipitation (GNIP) Database [dataset], 2015.

Irvalı, N., Galaasen, E. V., Ninnemann, U. S., Rosenthal, Y., Born, A., and Kleiven, H. F.: A low climate threshold for south Greenland Ice Sheet demise during the Late Pleistocene, Proceedings of the National Academy of Sciences, 117, 190-195, doi:10.1073/pnas.1911902116, 2020.

Jansen, E., Fronval, T., Rack, F., and Channell, J. E. T.: Pliocene-Pleistocene ice rafting history and cyclicity in the Nordic Seas during the last 3.5 Myr, Paleoceanography, 15, 709-721, https://doi.org/10.1029/1999PA000435, 2000.

Jensen, C. D.: Weather Observations from Greenland 1958-2024, Danish Meteorological Institute, 2025.

Johnsen, S. J., Clausen, H. B., Dansgaard, W., Gundestrup, N. S., Hammer, C. U., Andersen, U., Andersen, K. K., Hvidberg, C. S., Dahl-Jensen, D., Steffensen, J. P., Shoji, H., Sveinbjörnsdóttir, Á. E., White, J., Jouzel, J., and Fisher, D.: The δ18O record along the Greenland Ice Core Project deep ice core and the problem of possible Eemian climatic instability, Journal of Geophysical Research: Oceans, 102, 26397-26410, https://doi.org/10.1029/97JC00167, 1997.

Kjellman, S. E., Thomas, E. K., and Schomacker, A.: Arctic and sub-Arctic lake water δ2H and δ18O along a coastal-inland transect: Implications for interpreting water isotope proxy records, Journal of Hydrology, 607, 127556, https://doi.org/10.1016/j.jhydrol.2022.127556, 2022.

Kleinen, T., Hildebrandt, S., Prange, M., Rachmayani, R., Müller, S., Bezrukova, E., Brovkin, V., and Tarasov, P. E.: The climate and vegetation of Marine Isotope Stage 11 – Model results and proxy-based reconstructions at global and regional scale, Quaternary International, 348, 247-265, https://doi.org/10.1016/j.quaint.2013.12.028, 2014.

Kobashi, T., Menviel, L., Jeltsch-Thömmes, A., Vinther, B. M., Box, J. E., Muscheler, R., Nakaegawa, T., Pfister, P. L., Döring, M., Leuenberger, M., Wanner, H., and Ohmura, A.: Volcanic influence on centennial to millennial Holocene Greenland temperature change, Scientific Reports, 7, 1441, 10.1038/s41598-017-01451-7, 2017.

Koerner, R. and Russell, R. D.: δ18O variations in snow on the Devon Island ice cap, Northwest Territories, Canada, Canadian Journal of Earth Sciences, 16, 1419-1427, 10.1139/e79-126, 1979.

Konecky, B. L., McKay, N. P., Churakova, O. V., Comas-Bru, L., Dassié, E. P., DeLong, K. L., Falster, G. M., Fischer, M. J., Jones, M. D., Jonkers, L., Kaufman, D. S., Leduc, G., Managave, S. R., Martrat, B., Opel, T., Orsi, A. J., Partin, J. W., Sayani, H. R., Thomas, E. K., Thompson, D. M., Tyler, J. J., Abram, N. J., Atwood, A. R., Cartapanis, O., Conroy, J. L., Curran, M. A., Dee, S. G., Deininger, M., Divine, D. V., Kern, Z., Porter, T. J., Stevenson, S. L., von Gunten, L., and Iso2k Project, M.: The Iso2k database: a global compilation of paleo-δ18O and δ2H records to aid understanding of Common Era climate, Earth Syst. Sci. Data, 12, 2261-2288, 10.5194/essd-12-2261-2020, 2020.

Kusch, S., Bennike, O., Wagner, B., Lenz, M., Steffen, I., and Rethemeyer, J.: Holocene environmental history in high-Arctic North Greenland revealed by a combined biomarker and macrofossil approach, Boreas, 48, 273-286, https://doi.org/10.1111/bor.12377, 2019.

Larsen, H. C., Saunders, A. D., Clift, P. D., Beget, J., Wei, W., and Spezzaferri, S.: Seven Million Years of Glaciation in Greenland, Science, 264, 952-955, doi:10.1126/science.264.5161.952, 1994.

Larsen, N. K., Kjær, K. H., Lecavalier, B., Bjørk, A. A., Colding, S., Huybrechts, P., Jakobsen, K. E., Kjeldsen, K. K., Knudsen, K.-L., Odgaard, B. V., and Olsen, J.: The response of the southern Greenland ice sheet to the Holocene thermal maximum, Geology, 43, 291-294, 10.1130/g36476.1, 2015.

Lasher, G. E., Axford, Y., McFarlin, J. M., Kelly, M. A., Osterberg, E. C., and Berkelhammer, M. B.: Holocene temperatures and isotopes of precipitation in Northwest Greenland recorded in lacustrine organic materials, Quaternary Science Reviews, 170, 45-55, https://doi.org/10.1016/j.quascirev.2017.06.016, 2017.

Lawrence, K. T., Sosdian, S., White, H. E., and Rosenthal, Y.: North Atlantic climate evolution through the Plio-Pleistocene climate transitions, Earth and Planetary Science Letters, 300, 329-342, https://doi.org/10.1016/j.epsl.2010.10.013, 2010.

Lawrence, K. T., Herbert, T. D., Brown, C. M., Raymo, M. E., and Haywood, A. M.: High-amplitude variations in North Atlantic sea surface temperature during the early Pliocene warm period, Paleoceanography, 24, https://doi.org/10.1029/2008PA001669, 2009.

Lecavalier, B. S., Milne, G. A., Simpson, M. J. R., Wake, L., Huybrechts, P., Tarasov, L., Kjeldsen, K. K., Funder, S., Long, A. J., Woodroffe, S., Dyke, A. S., and Larsen, N. K.: A model of Greenland ice sheet deglaciation constrained by observations of relative sea level and ice extent, Quaternary Science Reviews, 102, 54-84, https://doi.org/10.1016/j.quascirev.2014.07.018, 2014.

Lee, J.-Y. M., J.; Bala, G.; Cao, L.; Corti, S.; Dunne, J.P.; Engelbrecht, F.; Fischer, E.; Fyfe, J.C.; Jones, C.; Maycock, A.; Mutemi, J.; Ndiaye, O.; Panickal, S.; Zhou, T.: Future Global Climate: Scenario-based Projections and Near-term Information, in: Climate Change 2021 – The Physical Science Basis: Working Group I Contribution to the Sixth Assessment Report of the Intergovernmental Panel on Climate Change, edited by: Masson-Delmotte, V. Z., P.; Pirani, A.; Connors, S.L.; Péan, C.; Berger, S.; Caud, N.; Chen, Y.; Goldfarb, L.; Gomis, M.I.; Huang, M.; Leitzell, K.; Lonnoy, E.; Matthews, J.B.R.; Maycock, T.K.; Waterfield, T.; Yelekçi, O.; Yu, R.; Zhou, B., Cambridge University Press, Cambridge, 553-672, 10.1017/9781009157896.006, 2023.

Majoube, M.: Fractionnement en oxygène 18 et en deutérium entre l’eau et sa vapeur, J. Chim. Phys., 68, 1423-1436, 1971.

Martin, K. C., Buizert, C., Brook, E., Williams, O. L., Edwards, J. S., Riddell-Young, B., Fudge, T. J., Mederbel, F., Beaudette, R., Severinghaus, J., Oyabu, I., Kawamura, K., Kirk, M., Koldtoft, I., Steffensen, J. P., and Blunier, T.: Greenland Ice Cores Reveal a South-To-North Difference in Holocene Thermal Maximum Timings, Geophysical Research Letters, 51, e2024GL111405, https://doi.org/10.1029/2024GL111405, 2024.

Martínez-Sosa, P., Tierney, J. E., Stefanescu, I. C., Dearing Crampton-Flood, E., Shuman, B. N., and Routson, C.: A global Bayesian temperature calibration for lacustrine brGDGTs, Geochimica et Cosmochimica Acta, 305, 87-105, https://doi.org/10.1016/j.gca.2021.04.038, 2021.

Martínez-Sosa, P., Tierney, J. E., Pérez-Angel, L. C., Stefanescu, I. C., Guo, J., Kirkels, F., Sepúlveda, J., Peterse, F., Shuman, B. N., and Reyes, A. V.: Development and Application of the Branched and Isoprenoid GDGT Machine Learning Classification Algorithm (BIGMaC) for Paleoenvironmental Reconstruction, Paleoceanography and Paleoclimatology, 38, e2023PA004611, https://doi.org/10.1029/2023PA004611, 2023.

McFarlin, J. M., Axford, Y., Kusch, S., Masterson, A. L., Lasher, G. E., and Osburn, M. R.: Aquatic plant wax hydrogen and carbon isotopes in Greenland lakes record shifts in methane cycling during past Holocene warming, Science Advances, 9, eadh9704, doi:10.1126/sciadv.adh9704, 2023.

McFarlin, J. M., Axford, Y., Osburn, M. R., Kelly, M. A., Osterberg, E. C., and Farnsworth, L. B.: Pronounced summer warming in northwest Greenland during the Holocene and Last Interglacial, Proceedings of the National Academy of Sciences, 115, 6357-6362, doi:10.1073/pnas.1720420115, 2018.

Melles, M., Brigham-Grette, J., Minyuk, P. S., Nowaczyk, N. R., Wennrich, V., DeConto, R. M., Anderson, P. M., Andreev, A. A., Coletti, A., Cook, T. L., Haltia-Hovi, E., Kukkonen, M., Lozhkin, A. V., Rosén, P., Tarasov, P., Vogel, H., and Wagner, B.: 2.8 Million Years of Arctic Climate Change from Lake El’gygytgyn, NE Russia, Science, 337, 315-320, doi:10.1126/science.1222135, 2012.

Miller, G. H., Alley, R. B., Brigham-Grette, J., Fitzpatrick, J. J., Polyak, L., Serreze, M. C., and White, J. W. C.: Arctic amplification: can the past constrain the future?, Quaternary Science Reviews, 29, 1779-1790, https://doi.org/10.1016/j.quascirev.2010.02.008, 2010.

Morlighem, M., Williams, C. N., Rignot, E., An, L., Arndt, J. E., Bamber, J. L., Catania, G., Chauché, N., Dowdeswell, J. A., Dorschel, B., Fenty, I., Hogan, K., Howat, I., Hubbard, A., Jakobsson, M., Jordan, T. M., Kjeldsen, K. K., Millan, R., Mayer, L., Mouginot, J., Noël, B. P. Y., O'Cofaigh, C., Palmer, S., Rysgaard, S., Seroussi, H., Siegert, M. J., Slabon, P., Straneo, F., van den Broeke, M. R., Weinrebe, W., Wood, M., and Zinglersen, K. B.: BedMachine v3: Complete Bed Topography and Ocean Bathymetry Mapping of Greenland From Multibeam Echo Sounding Combined With Mass Conservation, Geophysical Research Letters, 44, 11,051-011,061, https://doi.org/10.1002/2017GL074954, 2017.

Mostue, I. A., Hofer, S., Storelvmo, T., and Fettweis, X.: Cloud- and ice-albedo feedbacks drive greater Greenland Ice Sheet sensitivity to warming in CMIP6 than in CMIP5, The Cryosphere, 18, 475-488, 10.5194/tc-18-475-2024, 2024.

Naafs, B. D. A., Gallego-Sala, A. V., Inglis, G. N., and Pancost, R. D.: Refining the global branched glycerol dialkyl glycerol tetraether (brGDGT) soil temperature calibration, Organic Geochemistry, 106, 48-56, https://doi.org/10.1016/j.orggeochem.2017.01.009, 2017a.

Naafs, B. D. A., Inglis, G. N., Zheng, Y., Amesbury, M. J., Biester, H., Bindler, R., Blewett, J., Burrows, M. A., del Castillo Torres, D., Chambers, F. M., Cohen, A. D., Evershed, R. P., Feakins, S. J., Gałka, M., Gallego-Sala, A., Gandois, L., Gray, D. M., Hatcher, P. G., Honorio Coronado, E. N., Hughes, P. D. M., Huguet, A., Könönen, M., Laggoun-Défarge, F., Lähteenoja, O., Lamentowicz, M., Marchant, R., McClymont, E., Pontevedra-Pombal, X., Ponton, C., Pourmand, A., Rizzuti, A. M., Rochefort, L., Schellekens, J., De Vleeschouwer, F., and Pancost, R. D.: Introducing global peat-specific temperature and pH calibrations based on brGDGT bacterial lipids, Geochimica et Cosmochimica Acta, 208, 285-301, https://doi.org/10.1016/j.gca.2017.01.038, 2017b.

Nowicki, S. M. J., Payne, A., Larour, E., Seroussi, H., Goelzer, H., Lipscomb, W., Gregory, J., Abe-Ouchi, A., and Shepherd, A.: Ice Sheet Model Intercomparison Project (ISMIP6) contribution to CMIP6, Geosci. Model Dev., 9, 4521-4545, 10.5194/gmd-9-4521-2016, 2016.

Nusbaumer, J., Wong, T. E., Bardeen, C., and Noone, D.: Evaluating hydrological processes in the Community Atmosphere Model Version 5 (CAM5) using stable isotope ratios of water, Journal of Advances in Modeling Earth Systems, 9, 949-977, https://doi.org/10.1002/2016MS000839, 2017.

O'Connor, K. F., Berke, M. A., and Ziolkowski, L. A.: Hydrogen isotope fractionation in modern plants along a boreal-tundra transect in Alaska, Organic Geochemistry, 147, 104064, https://doi.org/10.1016/j.orggeochem.2020.104064, 2020.

Otiniano, G. A., Porter, T. J., Phillips, M. A., Juutinen, S., Weckström, J. B., and Heikkilä, M. P.: Reconstructing warm-season temperatures using brGDGTs and assessing biases in Holocene temperature records in northern Fennoscandia, Quaternary Science Reviews, 329, 108555, https://doi.org/10.1016/j.quascirev.2024.108555, 2024.

Paxman, G. J. G., Austermann, J., and Hollyday, A.: Total isostatic response to the complete unloading of the Greenland and Antarctic Ice Sheets, Scientific Reports, 12, 11399, 10.1038/s41598-022-15440-y, 2022.

Perner, K., Moros, M., Jennings, A., Lloyd, J., and Knudsen, K.: Holocene palaeoceanographic evolution off West Greenland, The Holocene, 23, 374-387, 10.1177/0959683612460785, 2013.

Raberg, J. H., de Wet, G. A., Geirsdóttir, Á., Sepúlveda, J., and Miller, G. H.: Oxygen Depletion in Lake Waters May Skew brGDGT-Inferred Temperatures by More Than 10°C, Geophysical Research Letters, 52, e2024GL113562, https://doi.org/10.1029/2024GL113562, 2025.

Raberg, J. H., Crump, S. E., de Wet, G., Harning, D. J., Miller, G. H., Geirsdóttir, Á., and Sepúlveda, J.: BrGDGT lipids in cold regions reflect summer soil temperature and seasonal soil water chemistry, Geochimica et Cosmochimica Acta, 369, 111-125, https://doi.org/10.1016/j.gca.2024.01.034, 2024.

Raberg, J. H., Harning, D. J., Crump, S. E., de Wet, G., Blumm, A., Kopf, S., Geirsdóttir, Á., Miller, G. H., and Sepúlveda, J.: Revised fractional abundances and warm-season temperatures substantially improve brGDGT calibrations in lake sediments, Biogeosciences, 18, 3579-3603, 10.5194/bg-18-3579-2021, 2021.

Raymo, M., Ruddiman, W. F., and Clement, B.: Pliocene-Pleistocene Paleoceanography of the North Atlantic at Deep Sea Drilling Project Site 609, Initial reports DSDP, Leg 94, Norfolk, Virginia to St. John's, Newfoundland. Part 2, 94, 895-901, 10.2973/dsdp.proc.94.125.1987, 1987.

Raymo, M. E., Ruddiman, W. F., Backman, J., Clement, B. M., and Martinson, D. G.: Late Pliocene variation in northern hemisphere ice sheets and North Atlantic deep water circulation, Paleoceanography, 4, 413-446, https://doi.org/10.1029/PA004i004p00413, 1989.

Reyes, A. V., Carlson, A. E., Beard, B. L., Hatfield, R. G., Stoner, J. S., Winsor, K., Welke, B., and Ullman, D. J.: South Greenland ice-sheet collapse during Marine Isotope Stage 11, Nature, 510, 525-528, 10.1038/nature13456, 2014.

Robinson, A., Alvarez-Solas, J., Calov, R., Ganopolski, A., and Montoya, M.: MIS-11 duration key to disappearance of the Greenland ice sheet, Nature Communications, 8, 16008, 10.1038/ncomms16008, 2017.

Sachse, D., Billault, I., Bowen, G. J., Chikaraishi, Y., Dawson, T. E., Feakins, S. J., Freeman, K. H., Magill, C. R., McInerney, F. A., Meer, M. T. J. v. d., Polissar, P., Robins, R. J., Sachs, J. P., Schmidt, H.-L., Sessions, A. L., White, J. W. C., West, J. B., and Kahmen, A.: Molecular Paleohydrology: Interpreting the Hydrogen-Isotopic Composition of Lipid Biomarkers from Photosynthesizing Organisms, Annual Review of Earth and Planetary Sciences, 40, 221-249, 10.1146/annurev-earth-042711-105535, 2012.

Schaefer, J. M., Finkel, R. C., Balco, G., Alley, R. B., Caffee, M. W., Briner, J. P., Young, N. E., Gow, A. J., and Schwartz, R.: Greenland was nearly ice-free for extended periods during the Pleistocene, Nature, 540, 252-255, 10.1038/nature20146, 2016.

Schneider, T., Castañeda, I. S., Zhao, B., Krüger, S., Salacup, J. M., and Bradley, R. S.: Tracing Holocene temperatures and human impact in a Greenlandic Lake: Novel insights from hyperspectral imaging and lipid biomarkers, Quaternary Science Reviews, 339, 108851, https://doi.org/10.1016/j.quascirev.2024.108851, 2024.

Schüpbach, S., Fischer, H., Bigler, M., Erhardt, T., Gfeller, G., Leuenberger, D., Mini, O., Mulvaney, R., Abram, N. J., Fleet, L., Frey, M. M., Thomas, E., Svensson, A., Dahl-Jensen, D., Kettner, E., Kjaer, H., Seierstad, I., Steffensen, J. P., Rasmussen, S. O., Vallelonga, P., Winstrup, M., Wegner, A., Twarloh, B., Wolff, K., Schmidt, K., Goto-Azuma, K., Kuramoto, T., Hirabayashi, M., Uetake, J., Zheng, J., Bourgeois, J., Fisher, D., Zhiheng, D., Xiao, C., Legrand, M., Spolaor, A., Gabrieli, J., Barbante, C., Kang, J. H., Hur, S. D., Hong, S. B., Hwang, H. J., Hong, S., Hansson, M., Iizuka, Y., Oyabu, I., Muscheler, R., Adolphi, F., Maselli, O., McConnell, J., and Wolff, E. W.: Greenland records of aerosol source and atmospheric lifetime changes from the Eemian to the Holocene, Nature Communications, 9, 1476, 10.1038/s41467-018-03924-3, 2018.

Shackleton, N. J., Backman, J., Zimmerman, H., Kent, D. V., Hall, M. A., Roberts, D. G., Schnitker, D., Baldauf, J. G., Desprairies, A., Homrighausen, R., Huddlestun, P., Keene, J. B., Kaltenback, A. J., Krumsiek, K. A. O., Morton, A. C., Murray, J. W., and Westberg-Smith, J.: Oxygen isotope calibration of the onset of ice-rafting and history of glaciation in the North Atlantic region, Nature, 307, 620-623, 10.1038/307620a0, 1984.

Sinninghe Damsté, J. S., Hopmans, E. C., Pancost, R. D., Schouten, S., and Geenevasen, J. A. J.: Newly discovered non-isoprenoid glycerol dialkyl glycerol tetraether lipids in sediments, Chemical Communications, 1683-1684, 10.1039/B004517I, 2000.

Smith, B., Fricker, H. A., Gardner, A. S., Medley, B., Nilsson, J., Paolo, F. S., Holschuh, N., Adusumilli, S., Brunt, K., Csatho, B., Harbeck, K., Markus, T., Neumann, T., Siegfried, M. R., and Zwally, H. J.: Pervasive ice sheet mass loss reflects competing ocean and atmosphere processes, Science, 368, 1239-1242, doi:10.1126/science.aaz5845, 2020.

Sodemann, H., Masson-Delmotte, V., Schwierz, C., Vinther, B. M., and Wernli, H.: Interannual variability of Greenland winter precipitation sources: 2. Effects of North Atlantic Oscillation variability on stable isotopes in precipitation, Journal of Geophysical Research: Atmospheres, 113, https://doi.org/10.1029/2007JD009416, 2008.

Sommers, A. N., Otto-Bliesner, B. L., Lipscomb, W. H., Lofverstrom, M., Shafer, S. L., Bartlein, P. J., Brady, E. C., Kluzek, E., Leguy, G., Thayer-Calder, K., and Tomas, R. A.: Retreat and Regrowth of the Greenland Ice Sheet During the Last Interglacial as Simulated by the CESM2-CISM2 Coupled Climate–Ice Sheet Model, Paleoceanography and Paleoclimatology, 36, e2021PA004272, https://doi.org/10.1029/2021PA004272, 2021.

St. John, K. E. K. and Krissek, L. A.: The late Miocene to Pleistocene ice-rafting history of southeast Greenland, Boreas, 31, 28-35, https://doi.org/10.1111/j.1502-3885.2002.tb01053.x, 2002.

Stuiver, M. and Grootes, P. M.: GISP2 Oxygen Isotope Ratios, Quaternary Research, 53, 277-284, https://doi.org/10.1006/qres.2000.2127, 2000.

Tabone, I., Robinson, A., Montoya, M., and Alvarez-Solas, J.: Holocene thinning in central Greenland controlled by the Northeast Greenland Ice Stream, Nature Communications, 15, 6434, 10.1038/s41467-024-50772-5, 2024.

Thomas, E., Briner, J., Ryan-Henry, J., and Huang, Y.: A major increase in winter snowfall during the middle Holocene on western Greenland caused by reduced sea ice in Baffin Bay and the Labrador Sea: Holocene Sea Ice Loss Caused More Snow, Geophysical Research Letters, 43, 10.1002/2016GL068513, 2016.

Thomas, E. K., Hollister, K. V., Cluett, A. A., and Corcoran, M. C.: Reconstructing Arctic Precipitation Seasonality Using Aquatic Leaf Wax δ2H in Lakes With Contrasting Residence Times, Paleoceanography and Paleoclimatology, 35, e2020PA003886, https://doi.org/10.1029/2020PA003886, 2020.

Thomas, E. K., Castañeda, I. S., McKay, N. P., Briner, J. P., Salacup, J. M., Nguyen, K. Q., and Schweinsberg, A. D.: A Wetter Arctic Coincident With Hemispheric Warming 8,000 Years Ago, Geophysical Research Letters, 45, 10,637-610,647, https://doi.org/10.1029/2018GL079517, 2018.

Thomas, E. K., Cluett, A. A., Erb, M. P., McKay, N. P., Briner, J. P., Castañeda, I. S., Corcoran, M. C., Cowling, O. C., Gorbey, D. B., Lindberg, K. R., Prince, K. K., and Salacup, J.: Early Holocene Laurentide Ice Sheet Retreat Influenced Summer Atmospheric Circulation in Baffin Bay, Geophysical Research Letters, 50, e2023GL103428, https://doi.org/10.1029/2023GL103428, 2023.

Tipple, B. J., Berke, M. A., Doman, C. E., Khachaturyan, S., and Ehleringer, J. R.: Leaf-wax <i>n</i>-alkanes record the plant–water environment at leaf flush, Proceedings of the National Academy of Sciences, 110, 2659-2664, doi:10.1073/pnas.1213875110, 2013.

Vinther, B. M., Buchardt, S. L., Clausen, H. B., Dahl-Jensen, D., Johnsen, S. J., Fisher, D. A., Koerner, R. M., Raynaud, D., Lipenkov, V., Andersen, K. K., Blunier, T., Rasmussen, S. O., Steffensen, J. P., and Svensson, A. M.: Holocene thinning of the Greenland ice sheet, Nature, 461, 385-388, 10.1038/nature08355, 2009.

Walcott-George, C. K., Balter-Kennedy, A., Briner, J. P., Schaefer, J. M., and Young, N. E.: Glacial erosion and history of Inglefield Land, northwestern Greenland, The Cryosphere, 19, 2067-2086, 10.5194/tc-19-2067-2025, 2025.

Wang, H., An, Z., Lu, H., Zhao, Z., and Liu, W.: Calibrating bacterial tetraether distributions towards in situ soil temperature and application to a loess-paleosol sequence, Quaternary Science Reviews, 231, 106172, https://doi.org/10.1016/j.quascirev.2020.106172, 2020.

Weidick, A. and Bennike, O.: Quaternary glaciation history and glaciology of Jakobshavn Isbræ and the Disko Bugt region, West Greenland: a review, GEUS Bulletin, 14, 1-78, 10.34194/geusb.v14.4985, 2007.

Zhang, W., Wang, Y., Smeets, P. C. J. P., Reijmer, C. H., Huai, B., Wang, J., and Sun, W.: Estimating near-surface climatology of multi-reanalyses over the Greenland Ice Sheet, Atmospheric Research, 259, 105676, https://doi.org/10.1016/j.atmosres.2021.105676, 2021.

Zhao, B., Castañeda, I. S., Bradley, R. S., Salacup, J. M., de Wet, G. A., Daniels, W. C., and Schneider, T.: Development of an in situ branched GDGT calibration in Lake 578, southern Greenland, Organic Geochemistry, 152, 104168, https://doi.org/10.1016/j.orggeochem.2020.104168, 2021.

Zhao, B., Russell, J. M., Tsai, V. C., Blaus, A., Parish, M. C., Liang, J., Wilk, A., Du, X., and Bush, M. B.: Evaluating global temperature calibrations for lacustrine branched GDGTs: Seasonal variability, paleoclimate implications, and future directions, Quaternary Science Reviews, 310, 108124, https://doi.org/10.1016/j.quascirev.2023.108124, 2023.